NUREG/CR-3613
PNL-4941
Vol. 3, No. 1

Evaluation of Welded and Repair-Welded Stainless Steel for LWR Service

Semiannual Report for
October 1984 Through March 1985

Prepared by D. G. Atteridge, S. M. Bruemmer, L. A. Charlot, R. E. Page

Pacific Northwest Laboratory
Operated by
Battelle Memorial Institute

Prepared for
U.S. Nuclear Regulatory Commission

NOTICE

This report was prepared as an account of work sponsored by an agency of the United States Government. Neither the United States Government nor any agency thereof, or any of their employees, makes any warranty, expressed or implied, or assumes any legal liability of responsibility for any third party's use, or the results of such use, of any information, apparatus, product or process disclosed in this report, or represents that its use by such third party would not infringe privately owned rights.

NOTICE

Availability of Reference Materials Cited in NRC Publications

Most documents cited in NRC publications will be available from one of the following sources:

1. The NRC Public Document Room, 1717 H Street, N.W.
   Washington, DC 20555
2. The Superintendent of Documents, U.S. Government Printing Office, Post Office Box 37082,
   Washington, DC 20013-7082
3. The National Technical Information Service, Springfield, VA 22161

Although the listing that follows represents the majority of documents cited in NRC publications, it is not intended to be exhaustive.

Referenced documents available for inspection and copying for a fee from the NRC Public Document Room include NRC correspondence and internal NRC memoranda; NRC Office of Inspection and Enforcement bulletins, circulars, information notices, inspection and investigation notices; Licensee Event Reports; vendor reports and correspondence; Commission papers; and applicant and licensee documents and correspondence.

The following documents in the NUREG series are available for purchase from the GPO Sales Program: formal NRC staff and contractor reports, NRC-sponsored conference proceedings, and NRC booklets and brochures. Also available are Regulatory Guides, NRC regulations in the *Code of Federal Regulations*, and *Nuclear Regulatory Commission Issuances*.

Documents available from the National Technical Information Service include NUREG-series reports and technical reports prepared by other federal agencies and reports prepared by the Atomic Energy Commission, forerunner agency to the Nuclear Regulatory Commission.

Documents available from public and special technical libraries include all open literature items, such as books, journal and periodical articles, and transactions. *Federal Register* notices, federal and state legislation, and congressional reports can usually be obtained from these libraries.

Documents such as theses, dissertations, foreign reports and translations, and non-NRC conference proceedings are available for purchase from the organization sponsoring the publication cited.

Single copies of NRC draft reports are available free, to the extent of supply, upon written request to the Division of Technical Information and Document Control, U.S. Nuclear Regulatory Commission, Washington, DC 20555.

Copies of industry codes and standards used in a substantive manner in the NRC regulatory process are maintained at the NRC Library, 7920 Norfolk Avenue, Bethesda, Maryland, and are available there for reference use by the public. Codes and standards are usually copyrighted and may be purchased from the originating organization or, if they are American National Standards, from the American National Standards Institute, 1430 Broadway, New York, NY 10018.

NUREG/CR-3613
PNL-4941
Vol. 3, No. 1
R5

Evaluation of Welded and Repair-Welded Stainless Steel for LWR Service

Semiannual Report for
October 1984 Through March 1985

Manuscript Completed: August 1985
Date Published: September 1985

Prepared by
D. G. Atteridge, S. M. Bruemmer, L. A. Charlot, R. E. Page

Pacific Northwest Laboratory
Richland, WA 99352

Prepared for
Division of Engineering Technology
Office of Nuclear Regulatory Research
U.S. Nuclear Regulatory Commission
Washington, D.C. 20555
NRC FIN B2449

ABSTRACT

Pacific Northwest Laboratory, under the sponsorship of the Division of Engineering Technology of the U.S. Nuclear Regulatory Commission, is conducting a program to determine a method for evaluating welded and repair-welded stainless steel (SS) piping for light-water reactor service. Validated models, based on experimental data, are being developed to predict microstructural development (e.g., the degree of sensitization) and the stress-corrosion cracking (SCC) resistance in the heat-affected zone of the SS weldments. Stress-corrosion cracking is caused by a combination of a susceptible microstructure, an aggressive environment, and tensile stress. Control of any of these three factors can eliminate SCC in most practical situations.

This program will measure and model the development of a susceptible microstructure as it pertains to welded and repair-welded SS pipe. Empirical correlations between material microstructure and SCC will be determined using constant extension rate tests. The successful completion of these tasks will result in a method for assessing the effects of welding/repairing parameters on the SCC resistance of component-specific nuclear reactor welds/repairs.

The present report describes the progress of these studies during the first half of the 1985 fiscal year.

SUMMARY

Pacific Northwest Laboratory, under the sponsorship of the Division of Engineering Technology of the U.S. Nuclear Regulatory Commission, is conducting a program to determine a method for evaluating welded and repair-welded stainless steel (SS) piping for light-water reactor service. Validated models, based on experimental data, are being developed to predict microstructure development (e.g., the degree of sensitization) and the stress-corrosion cracking (SCC) resistance in the heat-affected zone (HAZ) of the SS weldments. This program is measuring and modeling the development of a susceptible microstructure as it pertains to welded and repair-welded SS pipe. The successful completion of these tasks will result in a method for assessing the effects of welding/repairing parameters on the SCC resistance of component-specific nuclear reactor welds/repairs.

This report describes the progress of these studies during the first half of the 1985 fiscal year. Detailed temperature and strain histories have been monitored and are being analyzed as a function of distance through the HAZ of a 24-in.-dia Type 304 SS pipe weld. Sensitization development has been measured and modeled after both thermal and thermomechanical (TM) exposures, and the HAZ DOS has been mapped after each weld pass of the 24-in.-dia weld. Significant progress has been made in model development, enabling the prediction of DOS evolution in a large number of heats after isothermal, continuous-cooling, and actual welding TM exposures.

CONTENTS

FIGURES

TABLES

INTRODUCTION

Pacific Northwest Laboratory (PNL)[a] and the Division of Engineering Technology of the U.S. Nuclear Regulatory Commission (NRC) are conducting a program to determine a method for evaluating welded and repair-welded stainless steel (SS) piping for light-water reactor (LWR) service. Validated models based on experimental data are being developed to predict microstructural development (e.g., degree of sensitization) and the stress-corrosion cracking (SCC) resistance in the heat-affected zone (HAZ) of the SS weldments. The cumulative effects of material composition, past fabrication procedures, past service exposure, weldment thermomechanical (TM) history, and projected post-repair component life are being considered.

Austenitic SS components of commercial boiling-water (BWR) and pressurized water (PWR) reactors have experienced SCC in the HAZ of in-service SS welds. Although only a few instances of such cracking have been observed, their potential for causing serious component failure should not be underestimated. SCC is caused by a combination of a sensitized microstructure, an aggressive environment, and tensile stress. Control of any of these three factors can eliminate SCC in most practical situations.

This program will measure and model HAZ microstructural development as it pertains to welded and repair-welded SS pipe. Empirical correlations between material microstructure and SCC will be determined using constant extension rate tests (CERTs). The successful completion of these tasks will result in a method for assessing the effects of welding/repairing parameters on the SCC resistance of component-specific nuclear reactor welds/repairs.

Component-specific determination of microstructural development and SCC resistance for HAZs after welding/repairing requires a practical method for determining the fabrication history of the components. This program will use mill heat chemistries, in addition to the processing and fabrication records already required in the nuclear industry, for initial predictions. Recommendations for increased procedure controls and record changes will be made, as required, to obtain realistic predictions of SCC resistance.

The test matrix includes various Type 304, 304L, 304NG, 316, 316L, and 316NG SS materials used in nuclear reactor piping systems. The proposed program plan consists of the following phases:

Task I: Weld Thermomechanical History Determination

- experimental determination of the TM history of the HAZ on the pipe interior during primary and repair welds
- development of a HAZ TM history prediction method

(a) Operated for the U.S. Department of Energy (DOE) by Battelle Memorial Institute.

- experimental determination of HAZ microstructural development in fully characterized pipe welds and subsequent repair welds

Task II: Influence of Composition and Thermomechanical History on SCC

- experimental determination of the effects of bulk material composition and TM history on microstructural development and SCC susceptibility

- experimental efforts needed to determine the relationship between a given weld-induced microstructure and its susceptibility to SCC

Task III: SCC Prediction Methodology from Component-Specific Thermomechanical Histories

- development of a method to predict microstructural development (e.g., degree of sensitization) as a function of TM history

- development of a practical method for assessing the SCC susceptibility of the HAZ of component-specific welds/repairs.

Progress toward these goals in the first half of FY 1985 is presented in the following sections.

TASK I: WELD THERMOMECHANICAL HISTORY DETERMINATION

A weld/repair HAZ is subject to a complicated strain history superimposed over the heating and cooling cycle. Recent work indicates that this strain cycle increases the resultant sensitization of the HAZ over that predicted from strain-free isothermal data or that measured in specimens subjected to a similar but strain-free heating and cooling cycle. It is therefore necessary to precisely determine and duplicate the strain/temperature history of a HAZ for correct determination of the effect of welding on SCC susceptibility. The HAZ strain history is more complex in a multipass weld/repair than in a single-pass weld/repair. Strain history is also more complex in a pipe weld/repair than in a plate weld/repair where stresses can be relieved by plate bending, while circumferential restraint restricts metal movement in a pipe weld.

Previous experimentation involving the HAZ TM history concentrated on temperature measurements as a function of time and distance from the fusion line. The present work will determine simultaneously the strain and temperature history in welded/repaired pipe HAZs as a function of time and distance from the fusion line. It is expected that the resultant HAZ TM history will be a complex function of system restraint and heat absorption capability. Variables that can be expected to influence the TM history are pipe diameter and wall thickness, changes in wall thickness from one side of the fusion line to the other, depth of counterbore, weld/repair groove geometry, amount of weld crowning, weld heat input, length and depth of repair, and welding technique.

One goal of this task is to identify and measure the welding and repair-welding variables that have a major effect on resultant DOS, and to assess the ability to predict HAZ TM histories analytically. The initial work will be oriented toward experimentally determining HAZ TM histories of welds/repairs as a function of pipe size and heat input. These data will then be used to assess analytical methods for predicting TM histories of generic welds/repairs and the effect of specific welding and repair-welding variables on the resultant TM history.

The focus of the current experimental work is on the TM history of a thin layer on the inside surface of the pipe, as it is this region that controls IGSCC initiation. The placement of strain measurement devices and thermocouples on the pipe surface will allow real-time TM history measurement.

THERMOMECHANICAL HISTORY MEASUREMENTS ON A 24-IN.-DIA PIPE WELD

The thermomechanical history for a 24-in.-dia Type 304 SS Schedule 80 pipe weld is being monitored on a pass-by-pass basis. This is being done in order to generate a TM history data base for model development and assessment as well as to supply realistic TM cycles for use in weld simulation specimen testing. Degree of sensitization (DOS) measurements are being taken as a function of distance from the weld centerline between passes to allow determination of weld-induced microstructural changes.

Experimental Setup

The 24-in.-dia 304 SS pipe is being welded in the 2G position with the pipe axis oriented in the vertical direction. The welding technique is mechanized gas tungsten arc welding (GTAW) using an Astroarc 200-amp welding power supply (a Bechtel-modified Model E-200P) and welding head (Model AM-11) with the welding head traveling in a horizontal plane around the pipe, as illustrated in Figure 1. The welding head drive wheels ride in grooves machined in the pipe surface instead of the clamp-on segmented track that is normally used in field welding applications. This was done to control electrode movement out of the plane of the weld as the electrode travels around the pipe circumference. The out-of-plane movement using the clamp-on track was over 0.05 in., while it is less than 0.001 in. using the machined track.

The TM history data are being collected by a computer-based Data Retrieval and Analysis System (DRAS). The DRAS is capable of scanning 120 separate sensor channels and collecting a complete data set 25 times a second. The present configuration of the DRAS system is shown in Figure 2. The various TM history sensor signals are isolated and amplified before they enter the analog-to-digital converter portion of the DRAS in order to keep currents/voltages associated with welding away from the computer system.

The TM history sensors consist of chromel-alumel thermocouples, which are used to measure temperature changes, and modified commercial MTS fracture-toughness, crack-opening-displacement clip gages, which are used to measure

FIGURE 1. Monitoring of Thermomechanical History During Welding of 24-in.-dia Schedule 80 Type 304 SS Pipe

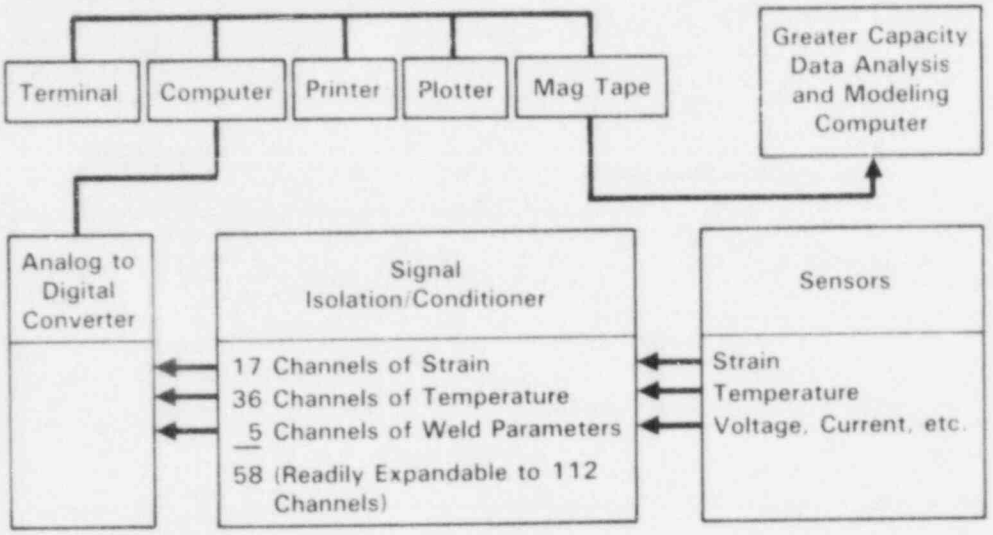

FIGURE 2. Schematic of the Data Retrieval and Analysis System Components

four different types of pipe deflections. For a more detailed discussion of these sensors see the 1984 Annual Report.(1)

A counterbore depth equal to twice the pipe wall thickness was machined into the inside surface of both sides of the pipe ends before weld joint preparation. The weld preparation used in the 24-in.-dia weld was a standard "narrow-gap" configuration used in GTAW of heavy-walled pipe as diagrammed in Figure 3. A land was used instead of a consumable insert ring to facilitate the placement of the various sensors as a function of distance from the weld centerline. The first half inch of wall thickness was machined as a 37.5° bevel from the vertical, while the rest of the wall was machined on a 10° bevel. All temperatures and inside pipe surface deflection measurements were confined to the counterbore surface area region.

Temperatures and strains are recorded as a function of arc-on-time and distance from the weld centerline. Counterbore surface strains are measured parallel and perpendicular to the weld. Surface deflections perpendicular to the plane of the counterbore and changes in concentricity of the pipe during welding are also monitored.

The counterbore surface had been separated into two instrumentation regions as a function of circumferential distance around the inside of the pipe. The first region consists of an instrument domain where surface temperature and strain measurements are taken. The second region consists of a DOS measurement area. Placement of the two regions around the pipe circumference is shown in Figure 4. Thermocouples are present in both regions while strain sensors are only present in the instrument domain region. The circumferential distance covered by the two regions is less than half the total circumference.

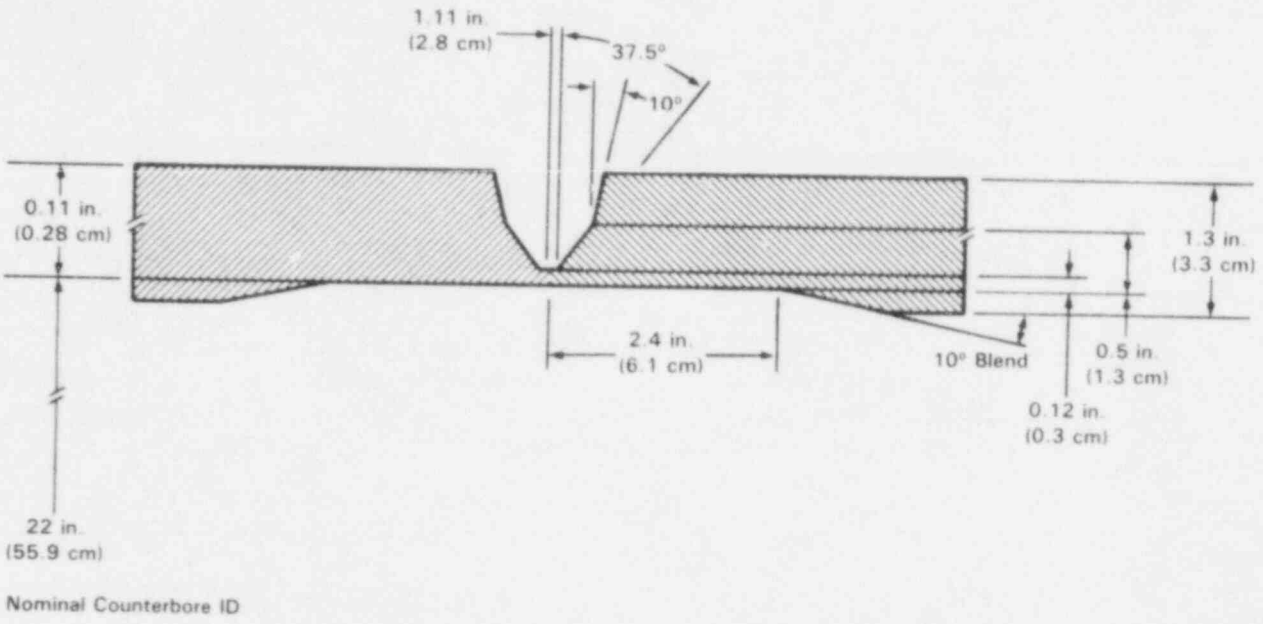

FIGURE 3. Groove Geometry of 24-in.-dia 304 SS Pipe Weld

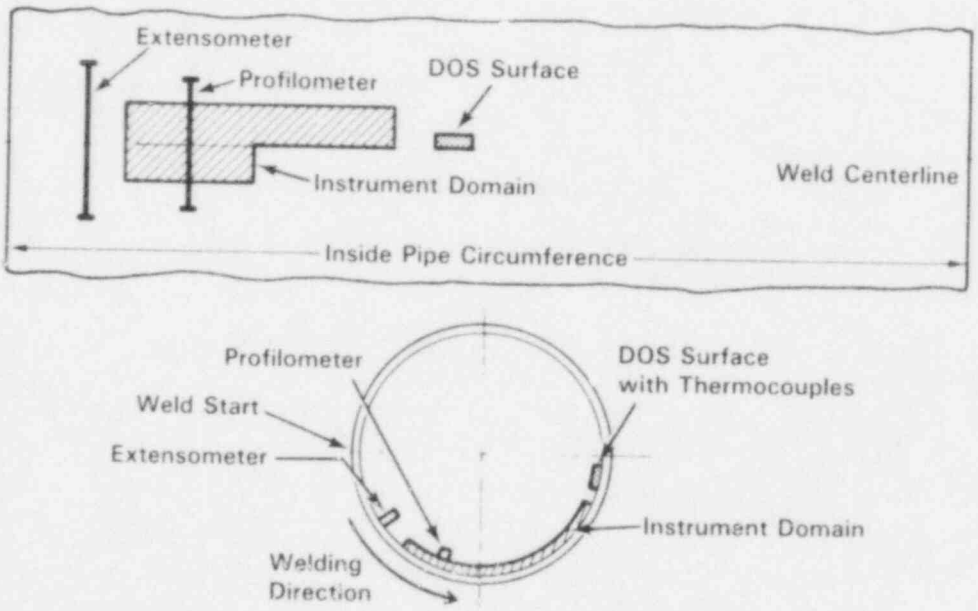

FIGURE 4. Layout of the Thermomechanical Sensors Around the Inside Surface of the 24-in.-dia 304 SS Pipe

The weld is started a considerable distance before the instrument domain. The first deflection monitor activated by the arc heated region is the extensometer. This gage monitors the overall axial expansion and contraction of the pipe in that region of the weld. A thermocouple monitors the surface temperature on the weld centerline directly beneath the extensometer.

The arc heat then encounters a series of surface strain-measurement gages and thermocouples as the arc continues around the pipe. The gages are attached to the surface by pairs of 1/8-in.-dia SS studs. A thermocouple is spot welded to the pipe surface between the studs to allow simultaneous monitoring of temperature and strain. A series of pairs of studs, oriented either parallel or perpendicular to the weld centerline, are attached to the counterbore surface (Figure 5a). A set of "feet" with knife edges for clip gage attachment are placed on each pair of studs. Modified crack-opening-displacement clip gages are then placed between the feet. Each modified clip gage consists of a standard MTS clip gage with ceramic leg extensions for thermal and electrical isolation. An external spring is placed over the outside edges of the feet to counteract the outward force exerted on the feet by the clip gage (Figure 5b).

A profilometer measures deflection perpendicular to the counterbore surface at six points on the counterbore surface. The profilometer is basically a bridge suspended over the weld HAZ with surface movement monitoring devices suspended from the bridge. One leg of a clip gage is attached to the stationary bridge while the other leg reacts to surface movement through a ceramic/metal stylus.

The DOS-measurement region has a line of thermocouples perpendicular to the weld centerline to allow subsequent DOS predictions. DOS readings are taken in this region as a function of distance from the weld centerline between each pass. The technique used in making these readings and the DOS measurement results are discussed in Task II. A comparison of the experimentally determined DOS results and the predicted DOS values is discussed in Task III.

TM History Measurements

The weld pass sequence of the first twelve weld passes is schematically represented in Figure 6a. The heat input used in these passes is presented in Figure 6b. The nominal fill per pass is also illustrated in these figures. The weight of weld filler metal used to achieve this fill is determined on a pass-by-pass basis and the resultant change in groove geometry due to each pass is recorded photographically after each pass. An example of the groove geometry changes observed after weld passes is shown in Figure 7, comparing the geometry before and after Pass 7. The figure also illustrates the welding electrode placement for the seventh and eighth pass as well as the resultant maximum temperature profiles achieved on the inside counterbore surface during these passes. Note that the maximum temperature profiles achieved agree well with the placement of the welding electrode before initiation of each pass.

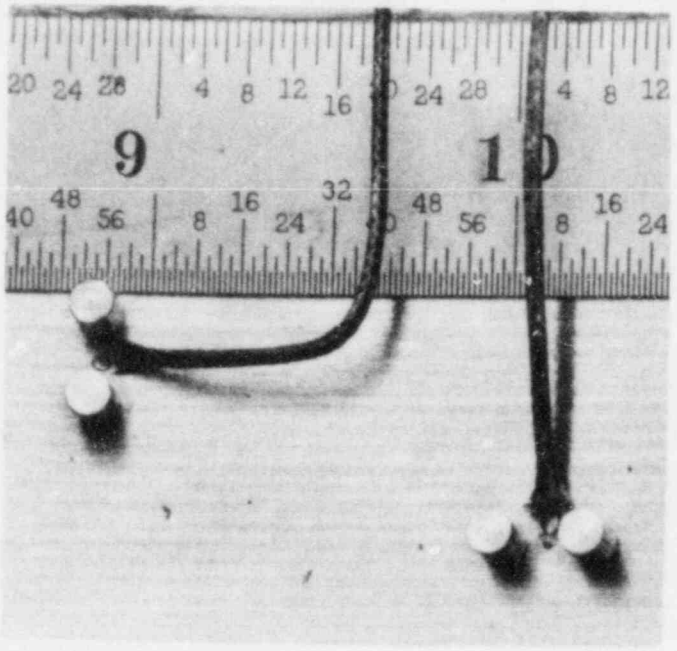

(a)

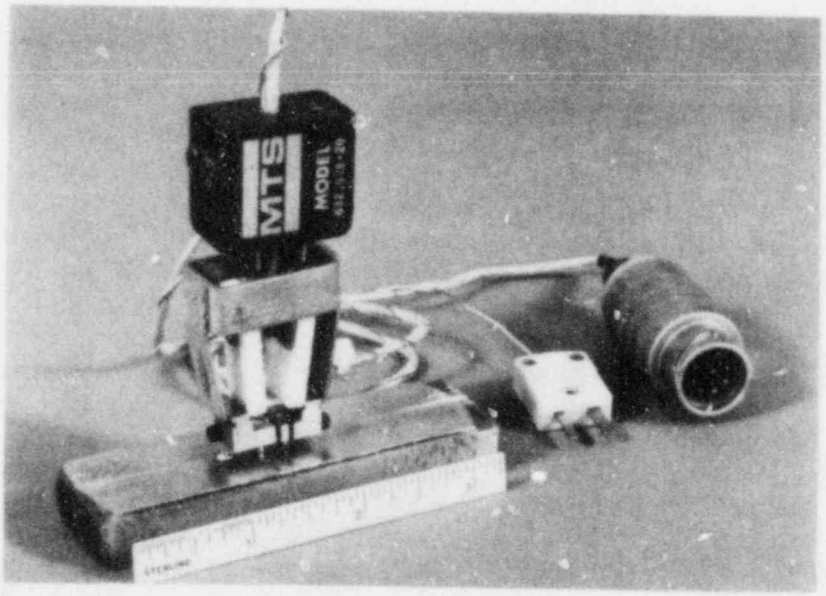

(b)

FIGURE 5. Surface Movement Monitoring Clip Gage Attachment Studs (a) and Completely Assembled Gage (b)

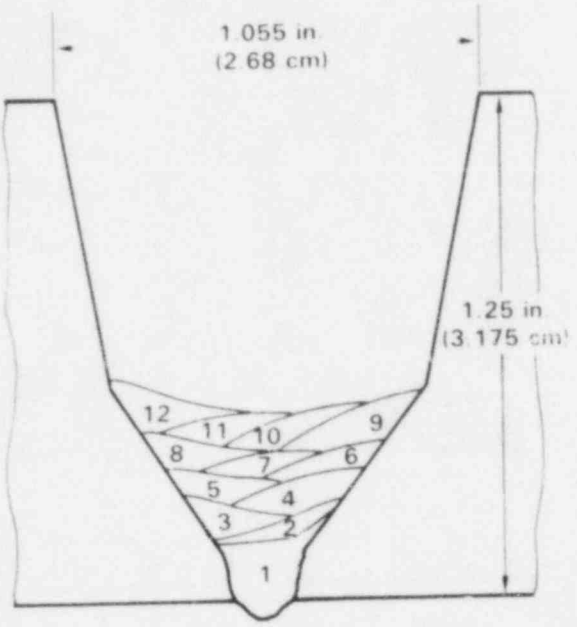

(a)

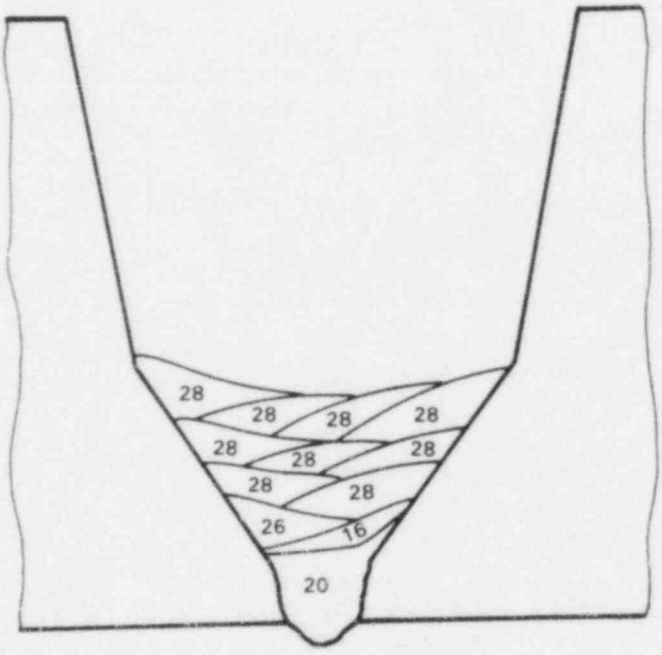

(b)

FIGURE 6. Weld Pass Sequence (a) and Heat Input Per Pass (b) for the First Twelve Passes of the 24-in.-dia Pipe

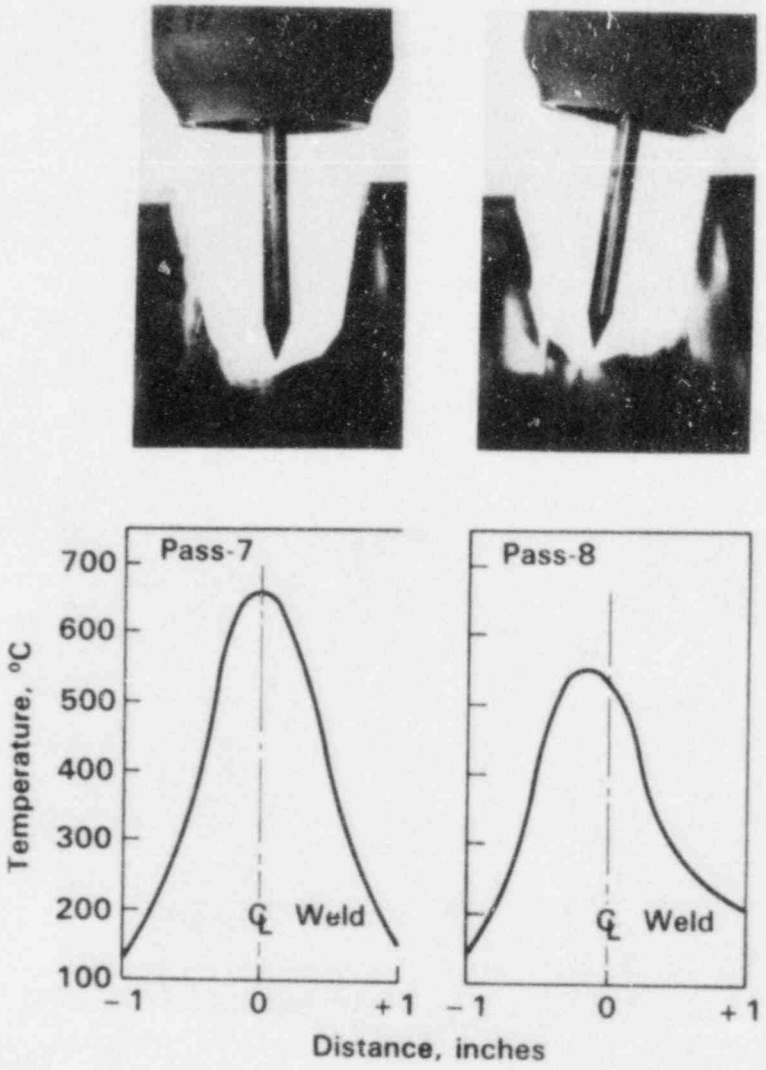

FIGURE 7. Weld-Induced Groove Geometry Changes and the Effect of Electrode Placement on Maximum Temperature Profiles

The extensometer gage documents the axial expansion or contraction taking place over the total length of pipe being welded. The post-pass gage readings indicate that considerable shrinkage took place during the first twelve weld passes, Figure 8a. It appears that the average weld contraction was 0.022 in. per pass for the first seven passes, after which it began tapering off. The total weld contraction after twelve passes was greater than 0.200 in. The groove fill and contraction taking place during the first twelve passes are illustrated in Figure 8b. Note that it appears that the contraction of the groove side walls is nominally parallel to the original groove side walls.

Weld contraction begins as soon as welding is initiated and before any measured temperature change in the instrument domain region. The instantaneous

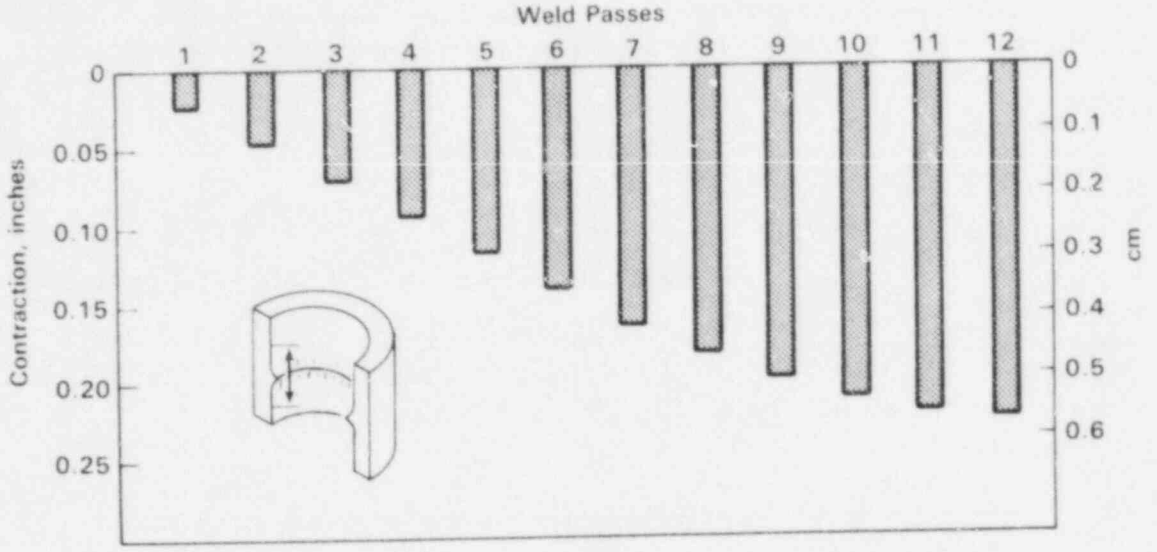

(a)

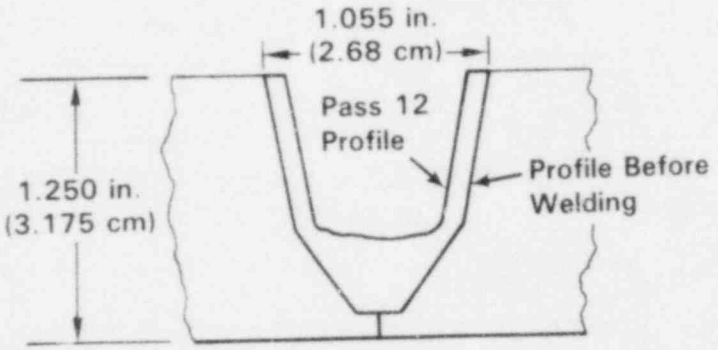

(b)

FIGURE 8. Cumulative Weld Region Contraction Perpendicular to the Weld Centerline as a Function of Weld Pass (a) and Changes in Weld Groove Geometry After 12 Weld Passes (b)

deformation seen by the extensometer gage, as a function of arc-on-time in Pass 12, along with the change in counterbore centerline temperature, measured directly beneath the gage, is shown in Figure 9. Most of the contraction takes place once the arc-induced temperature spike passes the gage. Contraction continues at a reduced rate as the arc travels around the pipe. A region of expansion is observed as the arc once again approaches the gage before the weld is terminated. Note that there is no appreciable temperature rise at the weld

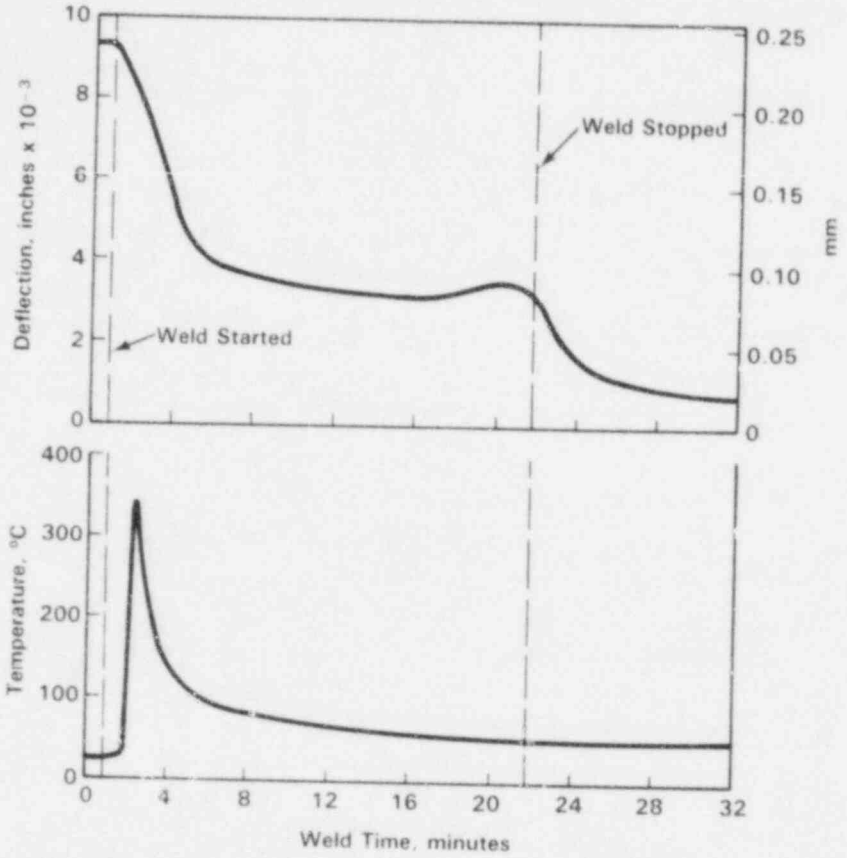

FIGURE 9. Axial Extensometer Displacement and Weld Centerline Temperature as a Function of Welding Time During Pass 12

centerline beneath the gage during this expansion and that an accelerated contraction takes place right after the arc is extinguished. This indicates that a "cold" deformation region extends several inches in front of the weld puddle.

Strain changes measured in the plane of the counterbore surface do not take place until the arc is close to the strain sensor position. A typical surface strain and temperature profile is shown in Figure 10 for a clip gage located 0.40 in. from the original weld centerline. The surface material is placed in compression before a measured temperature increase and goes into tension once a temperature begins to increase. The material then goes back into compression as the arc travels on. A permanent tension offset appears to be present after the pass is completed.

The magnitude of the strain change, as well as the maximum temperature, changes on a pass-by-pass basis in relationship to the position of the welding electrode. Temperature and strain profiles monitored 0.40 in. from the weld

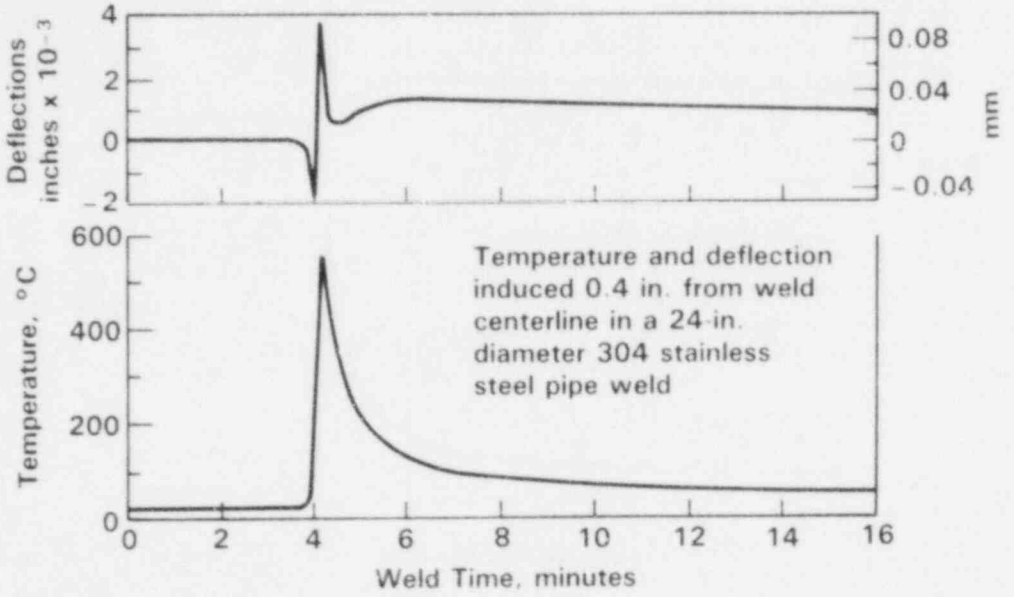

FIGURE 10. Temperature and Surface Deflection Parallel to the Weld Centerline Induced on the Counterbore Surface 0.40 in. from the Weld Centerline in Pass 3 of the 24-in.-dia Pipe Weld

centerline for the first twelve passes are presented in Figure 11. The absolute strain magnitude achieved during a weld pass and the tension offset appear to increase as the welding proceeds.

The post-pass counterbore surface movement detected by the profilometer gages indicates that the material near the weld continues to be upset and extrudes from the counterbore surface during at least the first twelve weld passes. The amount of localized counterbore diameter change and surface upsetting that was observed during the first twelve passes is illustrated in Figure 12. The original counterbore surface is defined as the straight line in the figure. The dotted contour illustrates the counterbore surface after four passes while the solid line illustrates the surface contour after twelve passes. It appears that the material very near the weld centerline undergoes plastic upsetting resulting in a net pipe diameter decrease while the material a little farther out undergoes plastic upsetting that results in a net increase in pipe diameter. It is assumed that the material farther out eventually blends into the original contour of the pipe.

The instantaneous counterbore surface movement measured under the profilometer during a given weld pass is a function of arc position (or welding time), as illustrated in Figure 13. The counterbore diameter appears to get larger once the arc is ignited. It then gets smaller as an arc-induced thermal bump travels under the profilometer styluses. Instantaneous pipe diameter increases as the thermal bump passes and then decreases as the arc continues to travel around the pipe. The magnitude of the detected surface change decreases with increasing distance from the weld centerline as illustrated in Figure 13.

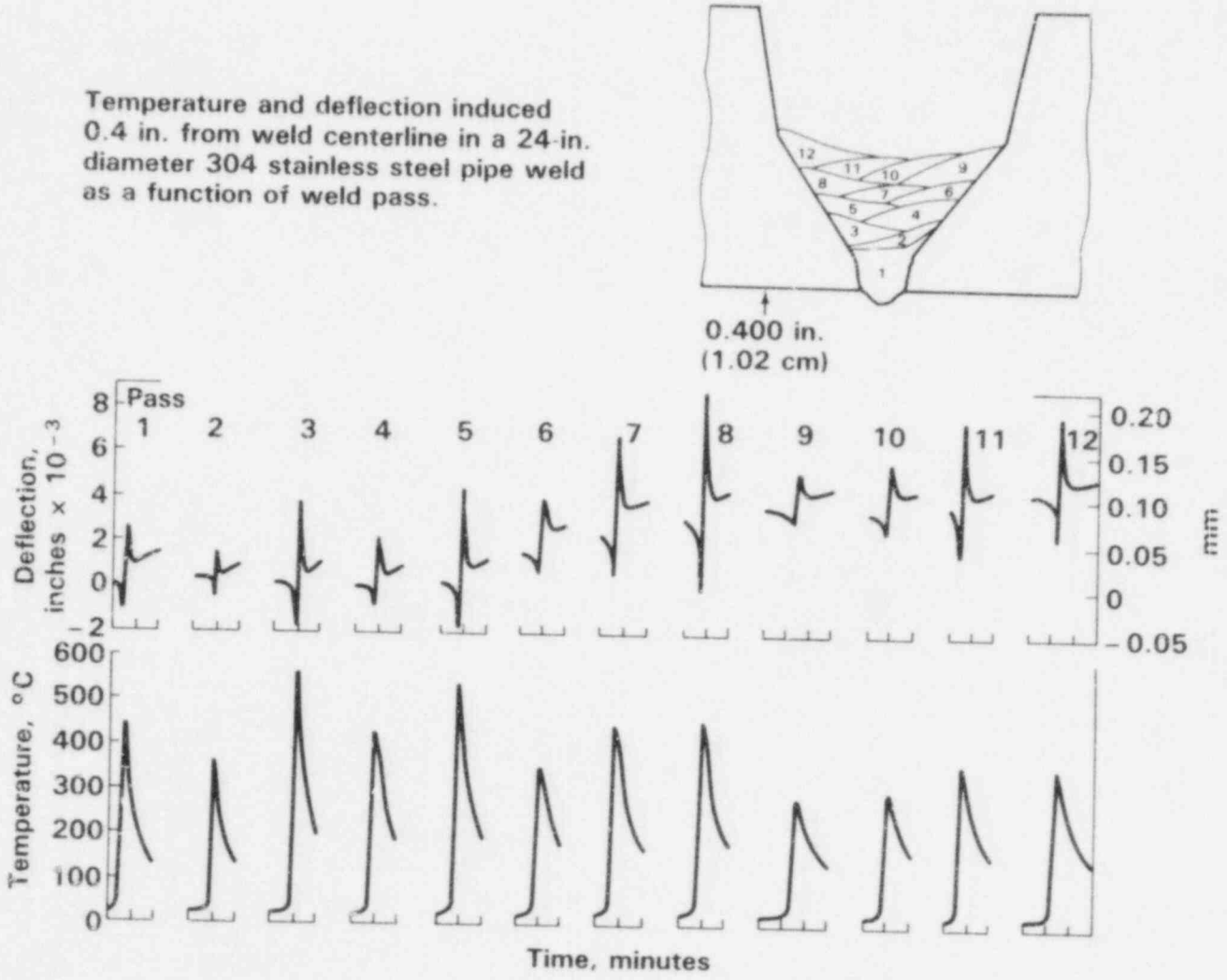

FIGURE 11. Temperature and Surface Deflection Parallel to the Weld Centerline Surface 0.40 in. from the Weld Centerline for the First Twelve Passes of the 21-in.-dia Pipe Weld

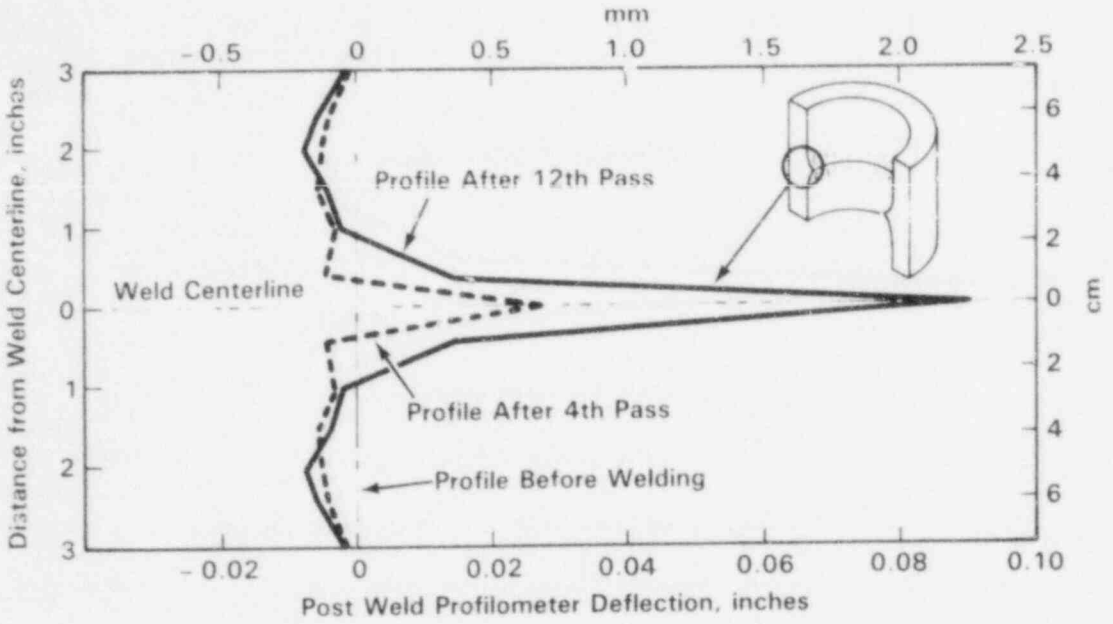

FIGURE 12. Post-Weld Pass Inside Counterbore Surface Profile for Passes 4 and 12

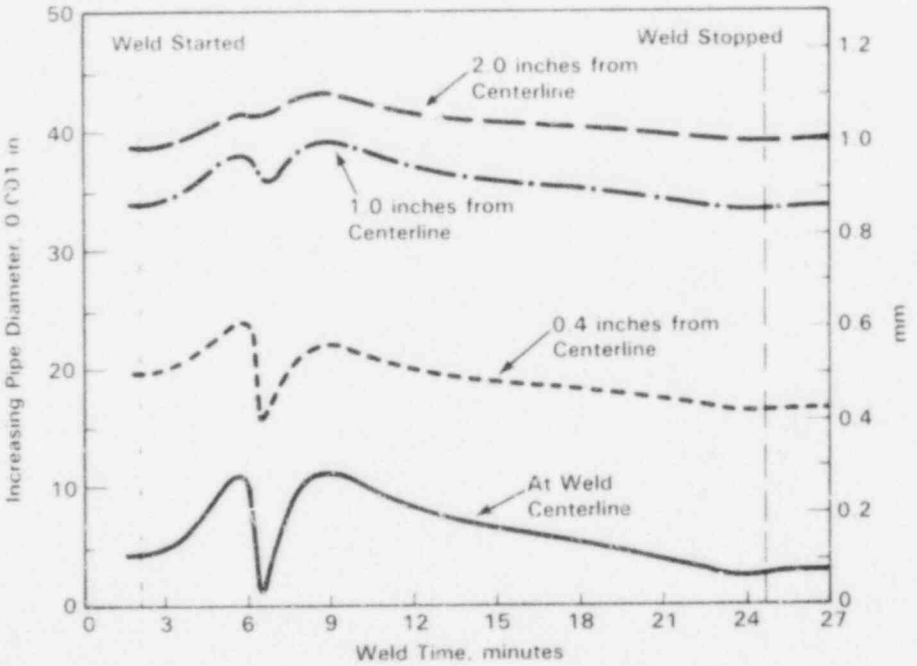

FIGURE 13. Deflection Measured Perpendicular to the Inside Counterbore Surface During Weld Pass 12 of the 24-in.-dia Pipe Weld as a Function of Distance from the Weld Centerline

The TM monitoring results reported above indicate that the TM history seen by the HAZ is a complex heating and simultaneous deformation process. They indicate that considerable plastic strain takes place during the weld thermal cycle and that both compressive and tensile plastic strain take place during welding. The strain difference measured between the start and the finish of the weld pass is of much smaller magnitude than the plastic deformation seen during the cycle. Plastic strain monitored during welding appears to be sufficient to substantially change the resultant weld-induced DOS from that expected from similar strain-free thermal cycling.

THERMOMECHANICAL HISTORY MODELING

A variety of techniques of predicting the TM history of the inside surface HAZ of a pipe weld are being evaluated. Thermal history prediction techniques range from simple closed form bead on (or in) plate solutions to sophisticated finite element modeling. Strain history models under consideration vary from finite element prediction models to experimentally determining cyclic strain for several pipe sizes and estimating all strain conditions from an experimental basis.

These various models will be evaluated for applicability and validity by comparing their predictive output to the data collected during welding of the 24-in.-dia pipe. Relevant models will be modified as required to yield a TM predictive capability that can be integrated with the microstructural change predictive model presently being developed as discussed in Task III.

TASK II: INFLUENCE OF COMPOSITION AND THERMOMECHANICAL HISTORY ON SCC

Austenitic SS may become sensitized and thus susceptible to SCC when chromium-rich carbides precipitate at grain interfaces, causing a chromium depletion of the adjacent matrix. This phenomenon is controlled by the thermodynamics of carbide formation and the kinetics of chromium diffusion. In a temperature regime where chromium carbide precipitation is thermodynamically stable (<850°C) and chromium diffusion is sufficiently rapid (>500°C), a SS can become sensitized in a relatively short time.

Stress-corrosion cracking of SS has been studied extensively for more than 20 years. However, much of the data that have been generated cannot be directly applied to the understanding and prediction of SCC in the HAZ. The development of a sensitized microstructure depends on a material's bulk composition and TM history. Neither of these factors, nor their effect on SCC, is sufficiently understood for accurate predictive modeling.

The primary objective of this task is to develop a sufficient data base to predict microstructural development (e.g., DOS) and SCC susceptibility as a function of TM history and material composition. Experimentation will involve weld simulation and small-diameter pipe weld parametric studies. Selected isothermal testing will also be conducted to gain a quantitative understanding of thermal and compositional effects on microstructural development. All data will be used in developing a microstructural development prediction methodology based on thermodynamic and kinetic models. Empirical correlations between material microstructure and SCC susceptibility will be determined in specific reactor-relevant environments to provide a basis for the SCC susceptibility prediction methodology.

MATERIALS

Approximately thirty heats of Type 304 or 316 SS have been obtained for isothermal, weld simulation and welding experimentation. Half of the program heats are in the form of 4-in.-dia pipe (Schedule 40 or 80). The majority of the experimental work is being performed on these pipe heats. Bulk compositions of the full matrix of program heats are listed in Table 1. Several of the carbon and nitrogen contents have been changed from those reported previously[1,2] to reflect additional chemical analyses.

EPR MEASUREMENTS OF SENSITIZATION DEVELOPMENT

Experimental Procedure

Specimens for analysis were metallographically prepared to a 1-μm diamond finish. Electrochemical potentiokinetic reactivation (EPR) tests were performed using an ISI Model WC-5 Metal Sensitization Detector. Test conditions have been reported previously.[1,2] A minimum of two tests were conducted on each specimen to determine DOS. Reported EPR-DOS values are normalized by the specimen area and grain size following the method outlined by Clarke.[3]

TABLE 1. Bulk Compositions and Grain Sizes of Program Pipe and Plate Heats

Heat[a]	Type	Composition, wt%										ASTM Grain Size[b]
		C	Cr	Ni	Mo	Mn	Si	P	S	N	B	
SS1	304L	0.013	18.21	10.34	0.07	1.54	0.58	0.012	0.008	0.039	0.001	4.4
SS2	304L	0.013	18.20	10.54	0.25	1.82	0.45	0.009	0.022	0.046	0.002	5
SS3	304L	0.019	18.30	10.33	0.20	1.51	0.45	0.012	0.001	0.018	0.001	5
SS4	304	0.044	18.35	9.18	0.31	1.63	0.36	0.012	0.001	0.049	0.002	7
SS5	304	0.054	18.42	8.47	0.08	1.01	0.53	0.012	0.011	0.062	0.001	6
SS6	304	0.050	18.67	8.78	0.16	1.89	0.38	0.012	0.002	0.059	0.001	6.5
SS7	304	0.060	19.17	9.54	0.12	1.31	0.42	0.013	0.015	0.041	0.001	4.5
SS11	316L	0.015	17.93	12.73	2.11	0.89	0.65	0.014	0.001	0.020	0.001	6
SS12	316L	0.014	17.77	12.64	2.18	0.89	0.60	0.014	0.005	0.023	0.001	6
SS13	316L	0.013	17.53	12.70	2.10	1.39	0.59	0.014	0.001	0.027	0.001	6
SS14	316L	0.020	16.92	12.90	2.30	1.66	0.38	0.014	0.002	0.011	0.001	6
SS15	316	0.035	17.32	10.91	2.15	1.71	0.63	0.013	0.012	0.062	0.002	4
SS16	316	0.058	17.11	11.43	2.26	1.77	0.41	0.014	0.005	0.008	0.002	7
SS17	316	0.067	16.81	11.21	2.20	1.46	0.28	0.016	0.020	0.071	0.003	4
C1	304L	0.016	18.55	8.91	0.14	1.81	0.46	0.019	0.004	0.083	--	4.5
C2	304L	0.020	18.38	9.03	0.23	1.65	0.51	0.033	0.009	0.067	--	6
C3	304	0.034	18.25	8.77	0.29	1.70	0.59	0.024	0.009	0.075	--	5.5
C4	304	0.052	18.16	8.26	0.19	1.72	0.77	0.018	0.006	0.088	--	4
C5	304	0.050	18.64	8.92	0.17	1.80	0.61	0.022	0.007	0.098	--	6
C6	304	0.062	18.48	8.75	0.20	1.72	0.39	0.013	0.013	0.065	--	4.5
C7	304	0.072	18.53	9.33	0.43	1.74	0.46	0.046	0.017	0.036	--	5
C10	316	0.050	17.40	12.50	2.17	1.30	0.66	0.032	0.018	--	--	3.5
N1	316L	0.011	16.50	10.18	2.06	1.67	0.62	0.030	0.013	0.086	--	4
N2	316L	0.019	16.20	10.35	2.15	1.70	0.42	0.030	0.013	0.087	--	4
N3	316LN	0.023	17.00	10.48	2.16	1.84	0.61	0.025	0.003	0.154	--	5.5
N4	316LN	0.014	16.80	10.34	2.16	1.63	0.59	0.026	0.009	0.145	--	4
N5	316LN	0.024	16.75	10.49	2.10	1.62	0.54	0.023	0.018	0.163	--	5.5
N6	316LN	0.012	16.63	10.60	2.10	1.69	0.52	0.022	0.006	0.190	--	5

(a) SS designation indicates pipe material, C and N designations indicate plate material.
(b) Grain sizes are for as-received, mill-annealed material.

All program heats listed in Table 1 were isothermally heat treated at temperatures ranging from 500 to 800°C and for times from 0.1 to 500 h. This data base has been used for preliminary correlations to model predictions.[1] Selected heats have also been evaluated after continuous-cooling heat treatments. Maximum temperatures of 800, 900 and 1000°C have been examined with cooling rates ranging from 0.02 to 5°C/s.

Isothermal Sensitization: Nitrogen Series

Sensitization development in the nitrogen series heats (N1 through N6) tracked reasonably well with bulk carbon content, and is consistent with the results for the other program heats reported earlier.[1,2] Nitrogen levels did not have a controlling influence on sensitization development within the range examined (0.08 to 0.20 wt%) in these heats. Examples of the time-temperature-DOS behavior for these materials are shown in Figure 14 for heat treatments at 600 and 700°C.

Degree of sensitization as measured by EPR increases with time at temperature. Heats with the higher carbon levels (N2, N3, and N5) reach significant EPR-DOS values (>15 C/cm^2) after 100 h at 700°C or 500 h at 600°C. Heats N4 and N6 with carbon levels of less than 0.015 wt% achieve EPR-DOS values of more than 10 C/cm^2 after 500 h at 600°C. This illustrates the fact that even very low-carbon materials (<0.02 wt%) can be sensitized using extreme heat treatments.

The effect of nitrogen content on sensitization development was evaluated by comparing Type 316L and 316LN heats with similar carbon contents. Three Type 316L pipe heats with relatively low nitrogen contents (0.02 to 0.027 wt%) are plotted along with three of the nitrogen series heats in Figure 15. All six of these heats have carbon contents between 0.011 and 0.015 wt%. Sensitization development in heats N4 and N6 is nearly identical to that for heats SS12 and SS13, even though the nitrogen series heats have about seven times the nitrogen content. These EPR data suggest that the additional nitrogen has little effect on sensitization development. However, more detailed examination of heat-treated specimen microstructures using analytical electron microscopy showed that nitrogen has a significant effect on grain boundary precipitation.

The primary grain boundary precipitates observed in Type 316L heats (such as SS12 and SS13) are $M_{23}C_6$ carbides. On the other hand, the Type 316LN heats exhibit both carbides ($M_{23}C_6$) and nitrides (Cr_2N) along grain boundaries as documented in Figure 16. The fact that sensitization development is similar between the Type 316L and 316LN heats may be the result of nitride formation that also contributes to sensitization. This may compensate for the inhibition of carbide precipitation by nitrogen. Several investigators[4-6] have shown that nitrogen reduces sensitization at levels up to about 0.12 wt%, but is not as effective at higher nitrogen contents. This is consistent with results for heat N1 (0.093 wt% N) where little sensitization was observed even after 500 h at 600°C (Figure 15).

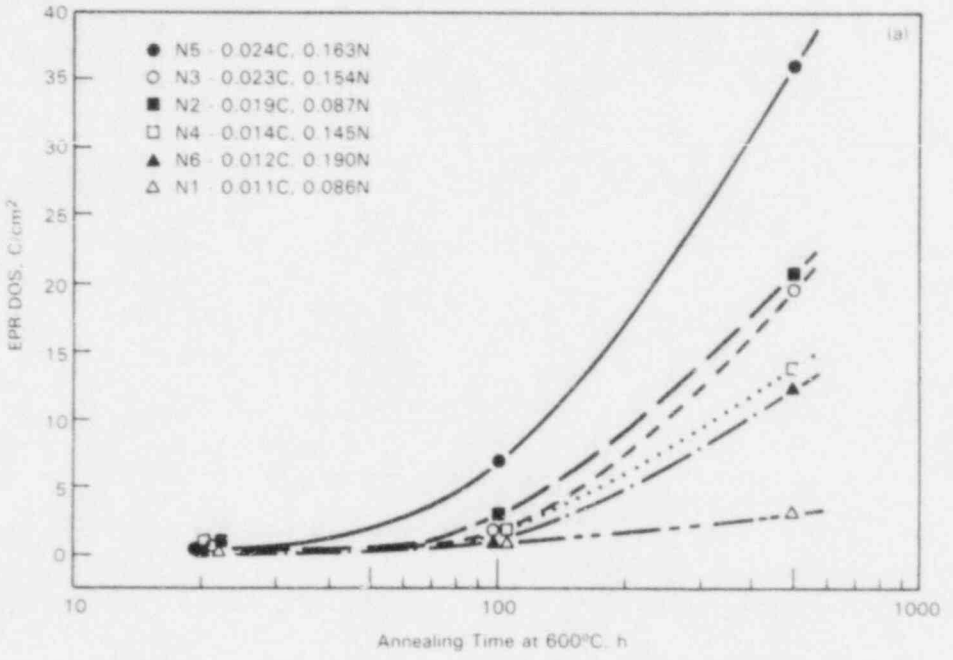

(a)

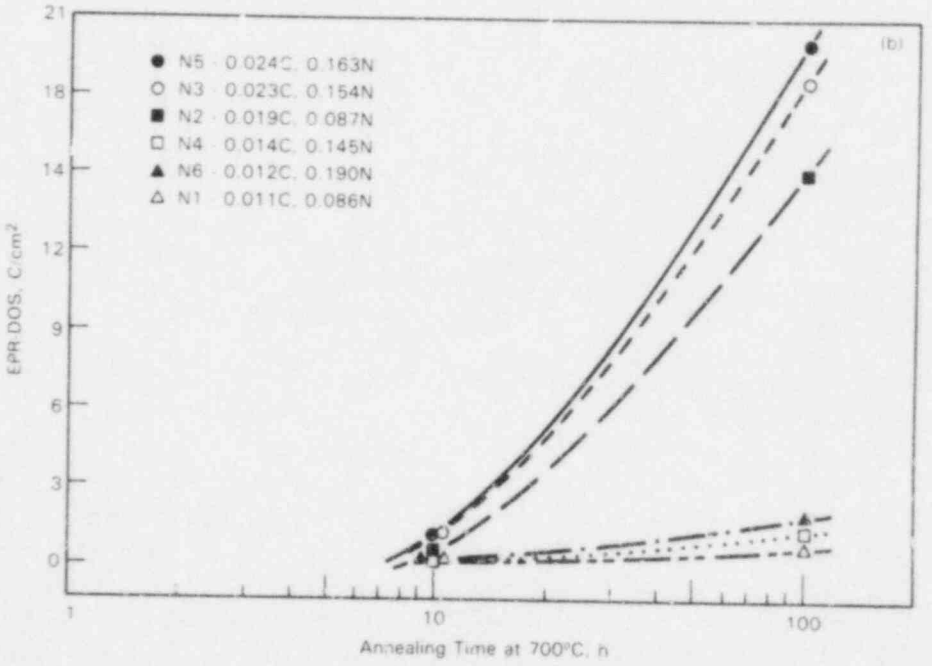

(b)

FIGURE 14. Sensitization Development in Type 316L and 316LN Heats at 600°C (a) and 700°C (b)

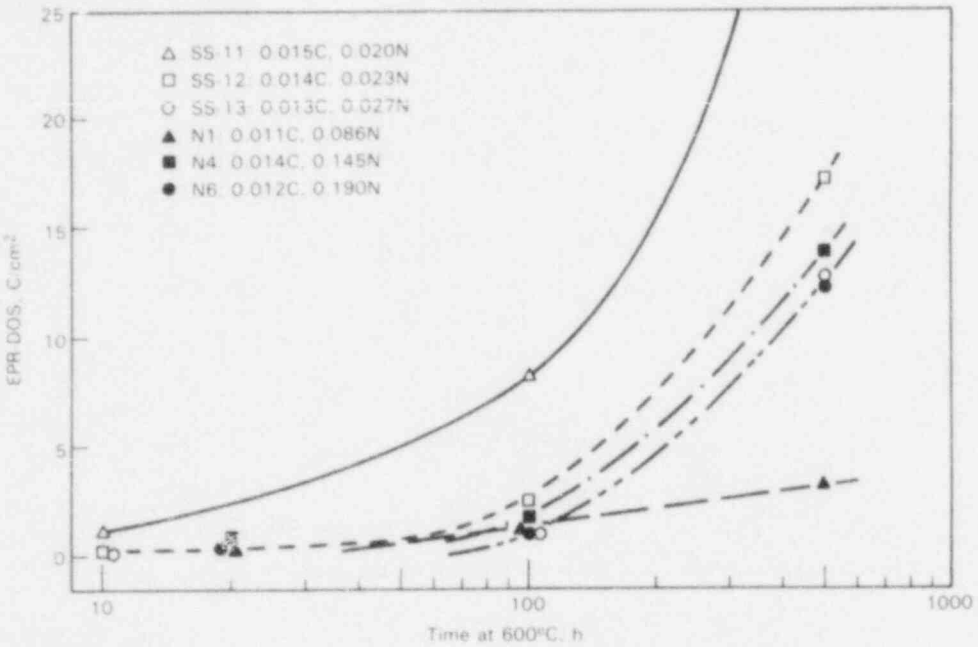

FIGURE 15. Comparison of Sensitization Development in Three "Low" Nitrogen and Three "High" Nitrogen Heats of Type 316 SS with Similar Carbon Contents

Sensitization develops more slowly in the higher-carbon, nitrogen series heats N2 and N3 than in heat SS13 as illustrated in Figure 17. Heat N5 exhibited DOS values comparable to those for SS13. This is probably due to increased nitride precipitation at grain boundaries. Although these results can be interpreted in line with previous work on nitrogen effects,[4-6] it is important to note that, by themselves, they do not show that nitrogen has a significant effect on sensitization.

Continuous-Cooling Sensitization

Eleven heats were selected for continuous-cooling testing after examination of the isothermal data. Five Type 304 SS (SS2, SS3, SS4, SS5, and SS7) and six Type 316 SS (SS13, SS14, SS15, SS16, N2, and N5) heats were examined. Preliminary experiments included three maximum temperatures (800, 900, and 1000°C) and three cooling rates (0.05, 0.5, and 2°C/s) from each maximum temperature.

The effect of bulk composition on sensitization development was generally similar to that indicated by isothermal testing. The importance of bulk composition, expressed as a composite chromium content,[7] is shown in Figure 18 for Types 304 and 316 SS heats after specific thermal exposures. The DOS during a particular thermal treatment is inversely related to the material chromium composite value. This type of relationship is also observed after isothermal sensitization.[1,2]

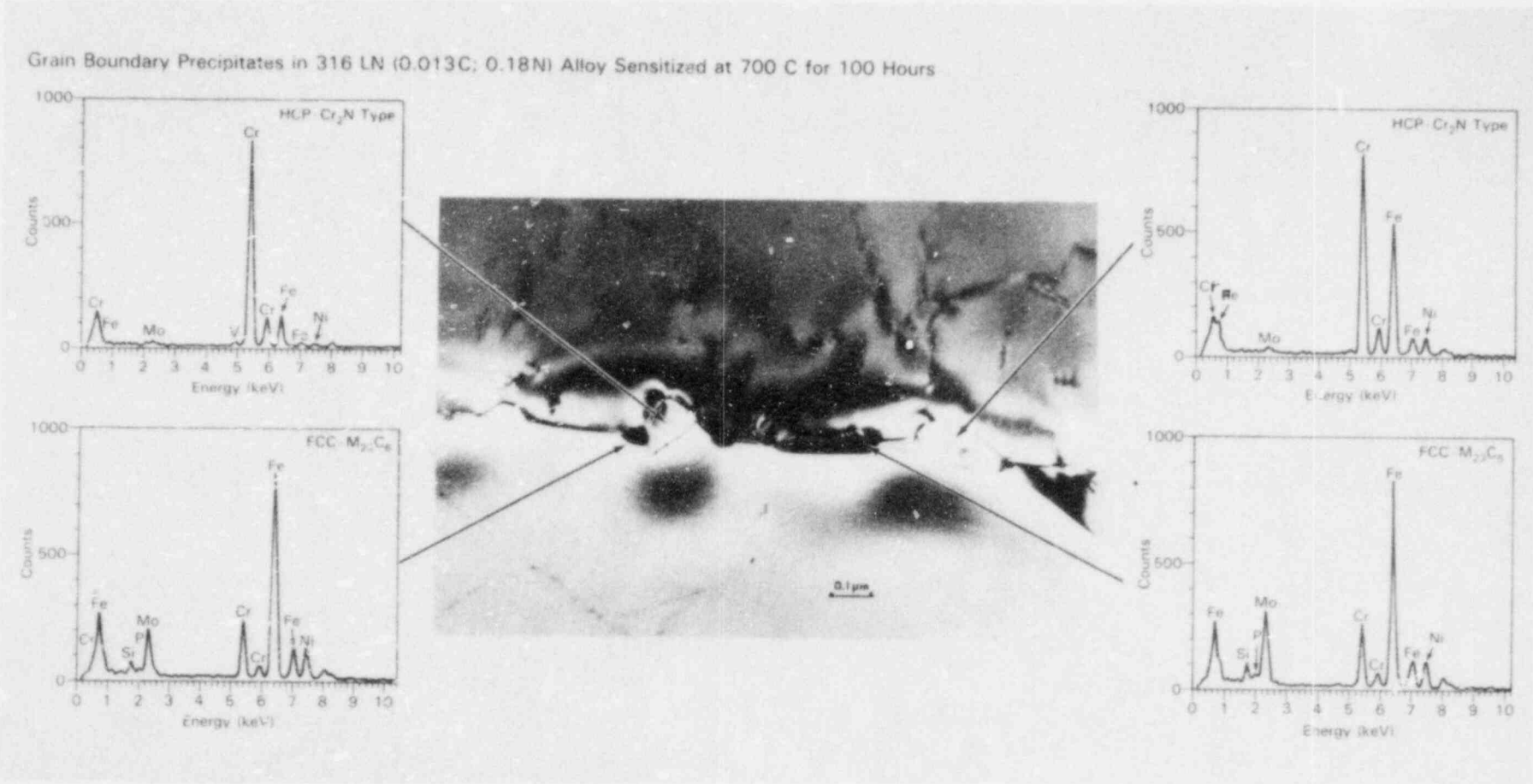

FIGURE 16. Identification of Grain Boundary Precipitates in Nitrogen-Series Heat N6 After a Heat Treatment of 100 h at 700°C

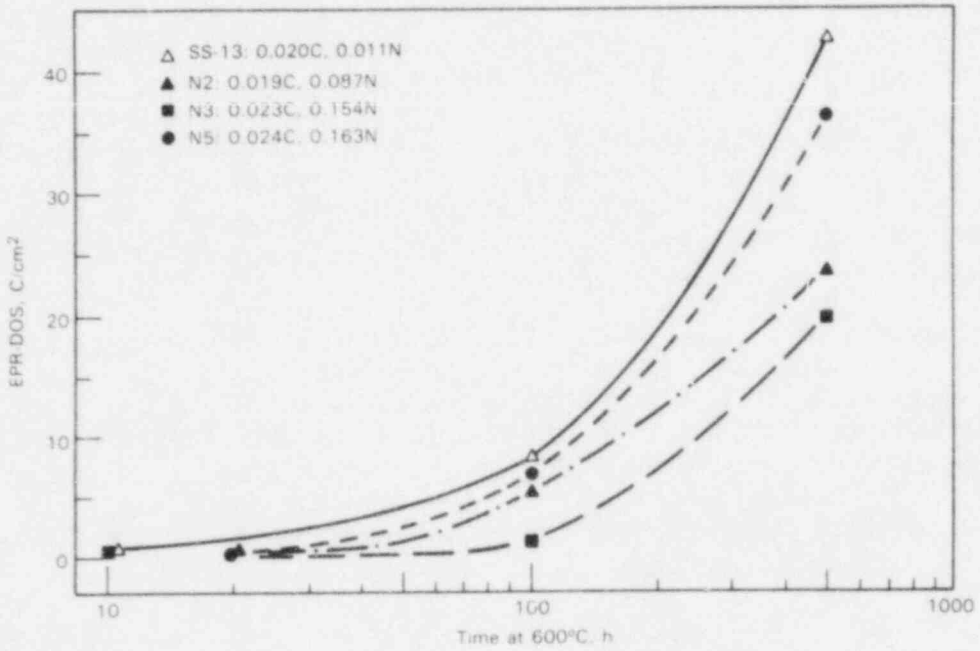

FIGURE 17. Comparison of Sensitization Development in a "Low" Nitrogen and Three "High" Nitrogen Heats of Type 316 SS with Similar Carbon Contents

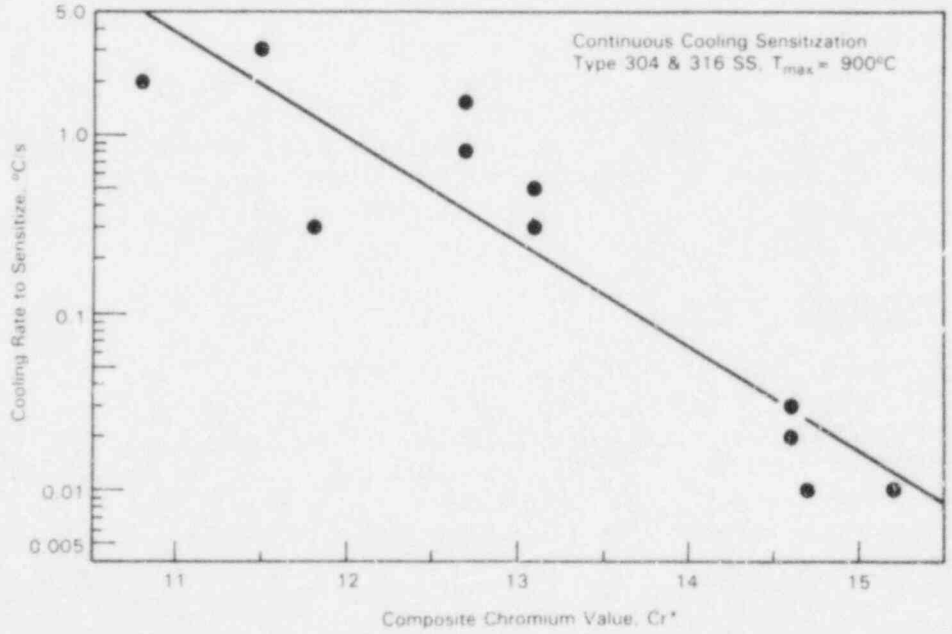

FIGURE 18. Measured DOS Developed After Specific Continuous-Cooling Treatments as a Function of a Heat's Chromium Composite Value Calculated from Bulk Composition (Cr* = Cr + 1.6 Mo - 0.2 Ni - 100 C)

Although the correlation between sensitization development and chromium composite exists for continuous-cooling sensitization data, the relative agreement was much better for isothermal sensitization data.[1,2] This is primarily due to differences in mill-annealed conditions among the heats tested. Differences in initial condition directly influence the time required for grain boundary carbide precipitation and the onset of sensitization. Because of the relatively short time at temperature where precipitate nucleation can occur during a continuous-cooling treatment, initial material condition is more important during continuous cooling than for an isothermal heat treatment to determine the extent of sensitization.

Sensitization development during continuous cooling depends on both the maximum temperature and the cooling rate. The effect of cooling rate on EPR-DOS is illustrated in Figure 19 for several Types 304 and 316 SS heats. In general, sensitization increases as the cooling rate decreases. An exception to this was observed when the maximum temperature was 1000°C. Measured EPR-DOS values were often lower after the slowest cooling rate (0.03°C/s) than the moderate cooling rate (0.6°C/s). Reasons for this reversal are not fully understood at this time. However, the initial mill-annealed condition is being removed during thermal treatments reaching 1000°C and may result in slower subsequent sensitization kinetics. Additional tests are under way at 950, 1000, and 1050°C to expand our data base and understanding of this aspect of continuous-cooling sensitization.

DIRECT MEASUREMENTS OF CHROMIUM DEPLETION

In order to model sensitization development, the first step required was to mathematically define those processes controlling sensitization, i.e., chromium carbide precipitation and development of a chromium-depleted zone. To ensure that the proper approach was implemented, a limited amount of direct measurements of chromium depletion at grain boundaries in Types 304 and 316 SS has been performed. A critical result of this work was the determination of empirical correlations between actual chromium depletion and DOS measurements by EPR. This was necessary to enable model verification based on a simple, inexpensive test (EPR).

Experimental Procedure

A Philips EM 400T scanning transmission electron microscope (STEM) equipped with an ultra-thin-window, energy-dispersive x-ray detector was used for microchemical analysis. Materials were mechanically and electrochemically thinned to less than 150 nm for examination and analysis. Quantification of x-ray spectra was made using the Cliff-Lorimer[8] technique, which relates x-ray intensities to elemental compositions through proportionality constants. Various materials and conditions have been examined, but most analyses have been conducted on heats C6 (Type 304 SS) and C10 (Type 316 SS). Compositions of these heats are given in Table 1. Specimens were solution annealed at 1100°C for 1 h, quenched and isothermally heat treated at temperatures between 500 and 800°C.

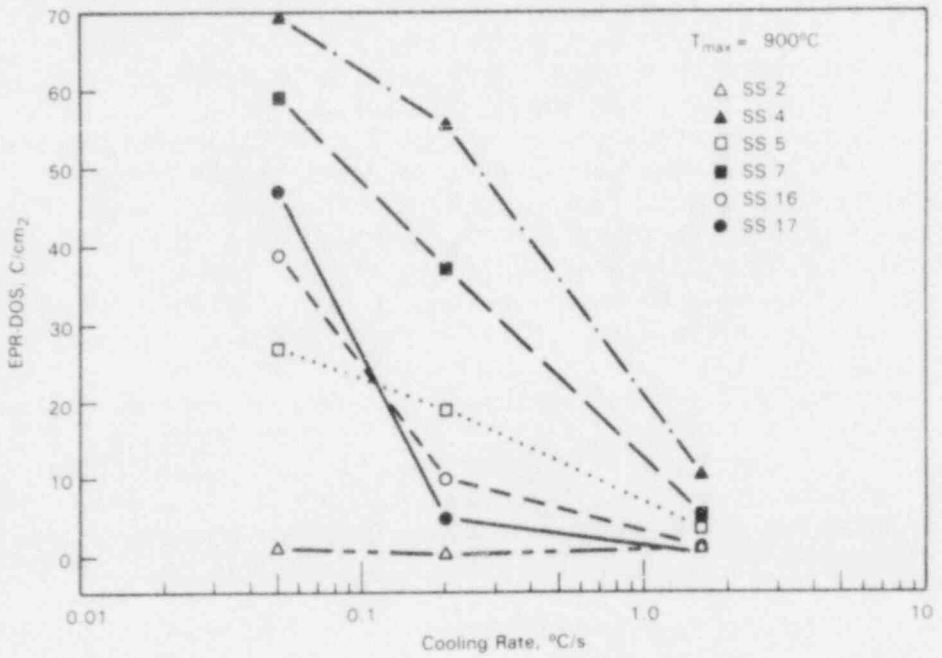

(a)

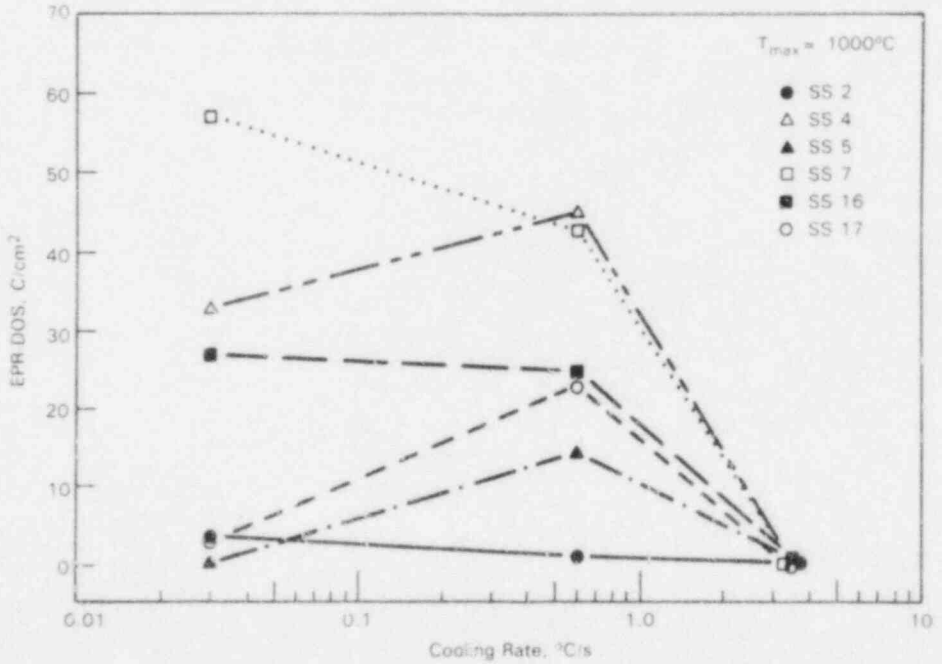

(b)

FIGURE 19. Continuous-Cooling Sensitization Results Showing the Effect of Cooling Rate on EPR Measured DOS for a Maximum Temperature of 900°C (a) and 1000°C (b)

Chromium-Depletion Measurements

Grain boundary chromium minimums and the widths of chromium-depleted zones were found to vary with heat treatment. The effect of heat treatment time on sensitization was examined for both materials at 700°C. Chromium-depletion width increased sharply as the annealing time was increased from 1 to 10 to 100 h as illustrated in Figure 20 and Table 2. Both alloys show only a narrow-chromium-depleted zone after 1 h which developed to an overall width of about one-half micron after 100 h. The density and size of carbides along grain boundaries also increased with heat treatment time. Typical carbide morphologies and regions of analysis between carbides are shown in Figure 21.

Chromium concentration gradients among the various carbide grain boundaries analyzed were reasonably consistent for a particular heat treatment. Only the least sensitized materials (700°C for 1 h) showed any significant (>20%) boundary-to-boundary variation. Results from grain boundary regions with the maximum depletion widths and minimum chromium concentrations are reported. Analyses of grain boundary regions a significant distance from carbide precipitates or those which showed evidence of boundary movement during annealing were not included in the comparison. Both of these regions exhibited chromium concentration distributions significantly different from those of "typical" boundaries.

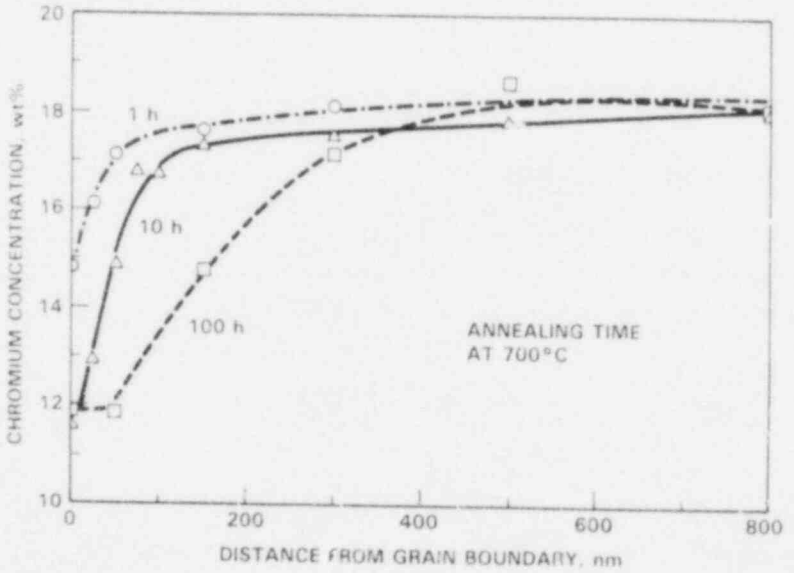

FIGURE 20. Typical Chromium Concentration Gradients in 304 SS After Heat Treatments at 700°C

TABLE 2. Minimum Grain Boundary Chromium Concentrations, Chromium-Depleted Zone Widths, and DOS Measured by EPR

Heat	Heat Treatment, °C/h	Minimum Grain Boundary Chromium Concentration, wt%	Depletion Width, nm Below 13% Cr	Depletion Width, nm Below 15% Cr	EPR-DOS, C/cm^2
C6	500/100	14.4	<10	20	16
(304 SS)	700/1 + 500/100	11.0	50	300	63
	600/100	11.4	30	100	46
	625/25	11.2	20	30	35
	700/1	12.5	10	20	14
	700/10	11.4	20	50	60
	700/100	11.9	100	320	82
	800/10	14.6	0	320	1
C10	600/100	11.7	60	180	51
(316 SS)	700/1	15.9	<5	<10	3
	700/10	10.4	50	120	35
	700/100	11.7	200	500	100
	800/10	11.9	100	250	35

No consistent variation in molybdenum concentration was observed as a function of distance from the grain boundary for the Type 316 heat. Although there was some indication of grain boundary depletion of molybdenum with increasing annealing time at 700°C, the depletion was less than 0.5 wt% and was not consistent on the boundaries examined. The additional analysis required to quantify the molybdenum concentration profiles was not performed in this study.

Specimens heat treated at other temperatures were evaluated to indicate the effect of annealing temperature on chromium depletion. The development of the chromium-depleted zone in the Type 304 alloy is considerably slower at 600 or 500°C than at 700°C, as evidenced by comparing results after 100-h anneals (Table 2). Chromium-depletion widths drop from ~500 nm at 700°C to ~100 nm at 600°C and to ~20 nm at 500°C. This change is consistent with the effect of temperature on chromium diffusivity.

The minimum grain boundary chromium concentration is another aspect of the chromium-depleted zone expected to change significantly with heat treatment temperature. As shown in Table 2, only a small decrease in chromium minimums was noted at temperatures lower than 700°C. The high value at 500°C after 100 h results from a profile too narrow to properly measure. The minimums measured at 600 and 625°C were not biased by this limitation. No grain boundaries or carbide interface regions were identified with chromium concentrations less than 10 wt% regardless of heat treatment conditions.

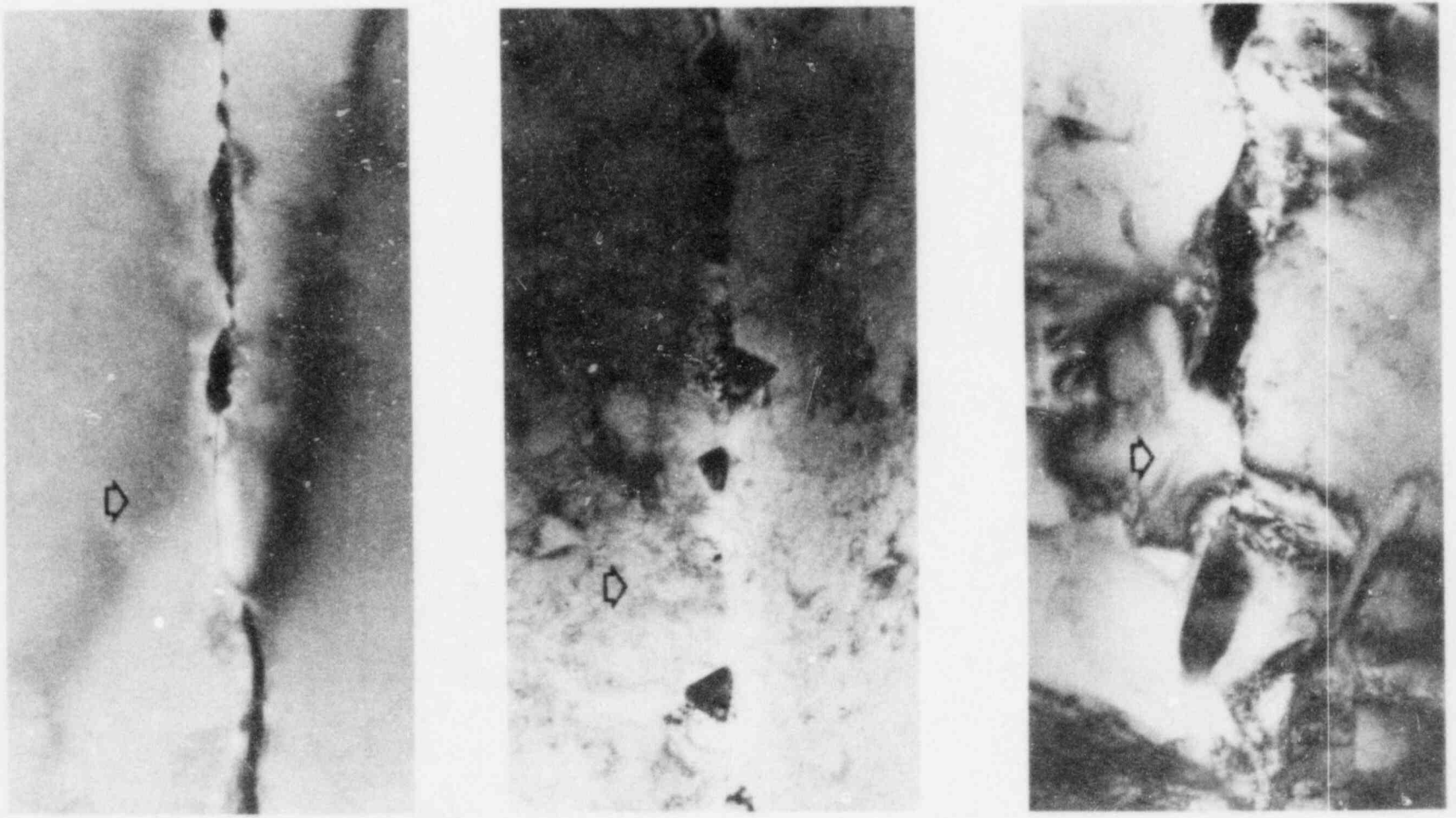

FIGURE 21. Micrographs Illustrating Typical Boundary Carbides in 304 SS Aged at 973K for (a) 1 h, (b) 10 h, and (c) 100 h. Chromium concentration gradients taken between particles as shown by arrows.

A decrease in minimum grain boundary chromium concentration with temperature can be seen by including the 800°C results. Minimums were more than 3 wt% lower in Type 304 specimens and about 1.5 wt% lower in Type 316 specimens when comparing the 700°C and 800°C results. In order to examine minimums at lower temperatures, a dual heat treatment of 700°C for 1 h plus 500°C for 100 h was given to the Type 304 heat. The 700°C heat treatment produced a high density of carbides along grain boundaries and enabled significant chromium depletion to develop during the 500°C anneal. Even though the depleted-zone width is quite large after the dual anneal (~300 nm), minimum grain boundary chromium levels remained near those measured after the 600 and 700°C heat treatments.

Comparison of Chromium-Depletion Measurements to EPR Measurements of DOS

If the EPR test predominantly attacks chromium-depleted regions within the austenitic stainless steel microstructure, then a correlation should exist between the chromium-depleted zone width and depth and EPR-DOS value. Examination of Table 2 indicates that significant depleted regions, particularly those below 13 wt%, produce large DOS values. The comparison between depletion and DOS also points out that moderate levels of sensitization (5 to 15 C/cm^2) result from very narrow depletion widths. The data from Table 2 have been combined with various other measurements on different heats in Figure 22 to illustrate the relationship between DOS and chromium-depletion width.

The comparison of EPR-DOS and chromium depletion by STEM-EDS indicates that both depletion width and depth control attack during the EPR tests. One might expect the volume of the depleted zone below some critical chromium level to best correlate to EPR results. While some reduction in data scatter can be seen comparing Figure 23 to Figure 22, the volume correlation does not show a significant improvement. The volume depletion parameter was calculated by determining the two-dimensional area of the region defined by the depletion width below 15 wt% and the minimum grain boundary chromium concentration.

Several reasons may account for the lack of a quantitative correlation between EPR and STEM-EDS measurements. The most important is that the available data base is not sufficient to make a more detailed comparison. Chromium depletion measured by STEM-EDS is documented on only a small number of grain boundaries. In obtaining these measurements, there is some variation in minimum chromium concentration and depletion width on different grain boundaries. This is particularly true for moderately sensitized specimens and for those heat treated at higher temperatures (>700°C). Carbide precipitation is not a homogeneous process and, as a result, precipitate density (and chromium depletion) can vary along individual boundaries and among different boundaries. Thus, the limited number of depletion profiles documented does not provide a quantitative basis for accurate correlation to EPR results.

STRAIN EFFECTS ON SENSITIZATION DEVELOPMENT

An important aspect of sensitization development in a weldment HAZ is the presence of simultaneous deformation during the welding cycle. In order to

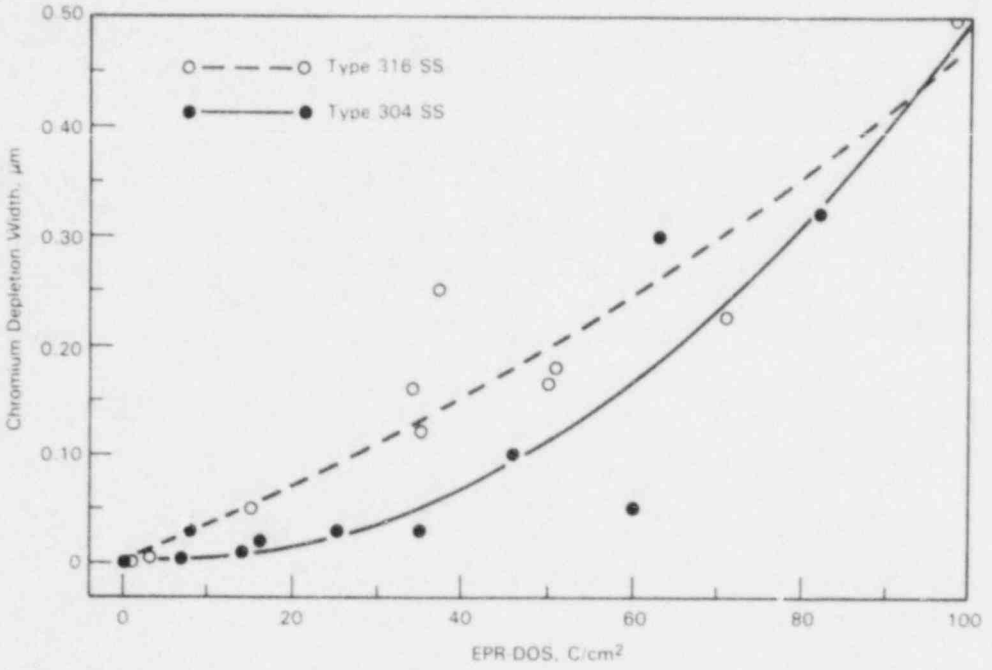

FIGURE 22. Correlation Between DOS Measured by EPR and Width of Chromium-Depleted Zone Measured by STEM-EDS

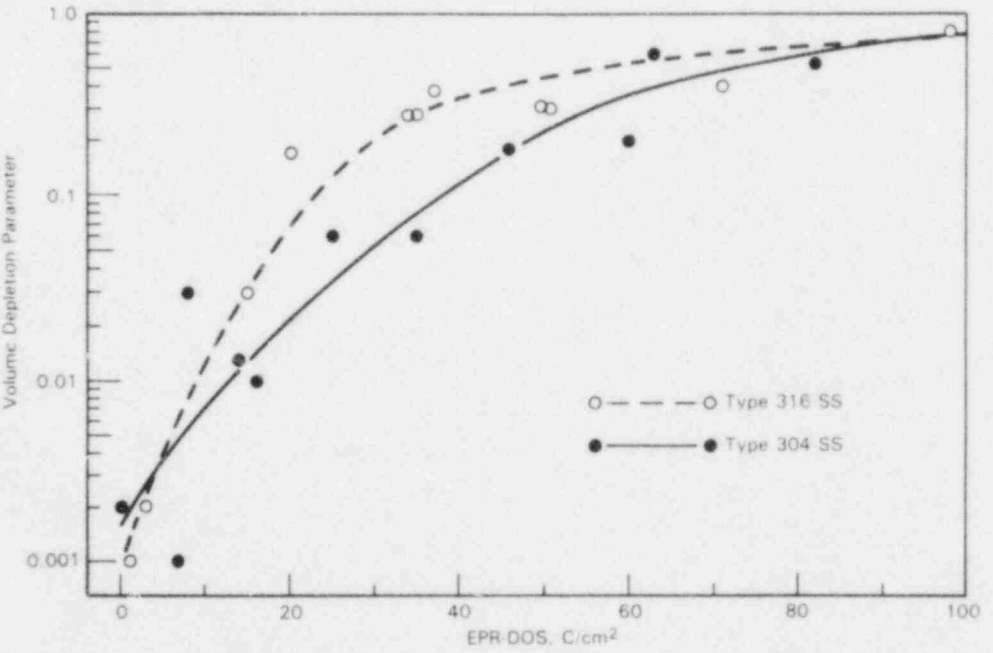

FIGURE 23. Correlation Between DOS Measured by EPR and Volume of Chromium-Depleted Zone Measured by STEM-EDS

generate an adequate data base for the understanding and modeling of HAZ sensitization, a series of experiments are continuing to determine strain effects on sensitization development. The effect of uniaxial straining during isothermal heat treatments has been investigated using flat tensile specimens strained at constant rates during additive isothermal exposures. Control (unstrained) specimens are attached to the gage region of the tensile specimen and heat treated simultaneously. DOS measurements are taken after each exposure using the field cell EPR technique. Typical isothermal cycles have been 0.5 or 1 h at 600°C for the first several cycles. Longer exposures are then used to achieve a total test time of 9 h.

A significant acceleration in sensitization kinetics has been documented due to the presence of simultaneous deformation on several Type 304 SS heats. Measurable sensitization is observed in shorter times, and DOS reaches high values during the additive cycles in strained versus unstrained specimens. Examples of sensitization development as a function of heat treatment time are shown in Figure 24. Significant sensitization is observed after 1 h in the strained specimens, whereas a comparable level is not reached in the unstrained specimens, even after 9 h. Most grain boundaries are attacked in the EPR test in the strained specimen after only one hour indicating a continuous grain boundary depletion zone. The unstrained specimen shows only attack on isolated grain boundary sections.

Strained and unstrained specimens of heat C7 were examined by TEM and STEM-EDS techniques after the final additive thermal cycle. Bright and dark field micrographs are presented in Figure 25. These show typical microstructures at relatively high magnification. The accumulated damage (i.e., dislocation density) as a result of the simultaneous deformation of 6% strain per hour is obvious in the bright field image. Another apparent difference between strained and unstrained specimens is the shape of the carbide precipitates. They are elongated along the boundary in the unstrained material and extend preferentially into one grain in the strained material. Not all boundaries exhibit this appearance in the strained specimen, but a significant percentage do. It is possible that only boundaries that were properly oriented to the applied stress undergo this carbide growth pattern.

Chromium depletion was much more pronounced in the strained than in the unstrained material as shown in Figure 26. Minimum chromium levels on the strained specimen were found to be close to 8 wt% compared to about 13 wt% in the unstrained specimen. No chromium depletion below 9.5 wt% has been observed in any of the isothermally heat-treated specimens. Simultaneous strain appears to have a dramatic effect on both the thermodynamics and kinetics of sensitization. Another aspect of the chromium-depletion profiles in the strained specimen is that the depletion profile is not symmetric around the grain boundary (as is generally the case for unstrained specimens). Minimum chromium levels are observed to be tens of nanometers from the boundary in grains where carbides are extended. These observations give some insight into the considerable effect that simultaneous plastic deformation has on sensitization development. Experiments are continuing to isolate the mechanism(s) for the increase in sensitization kinetics. Grain boundary movement during thermomechanical treatment may play an important role in this process.

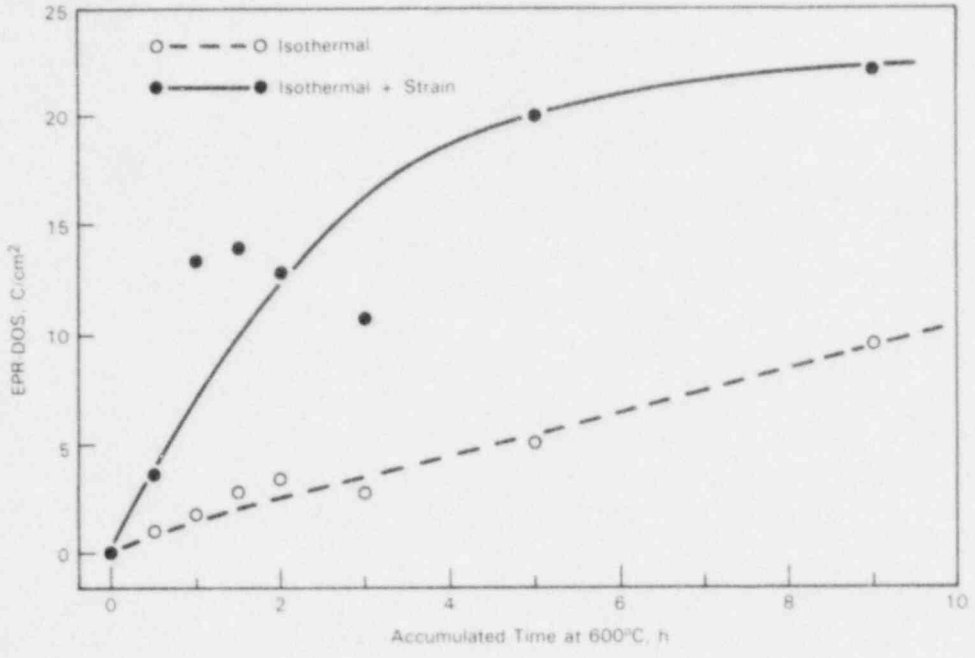

(a)

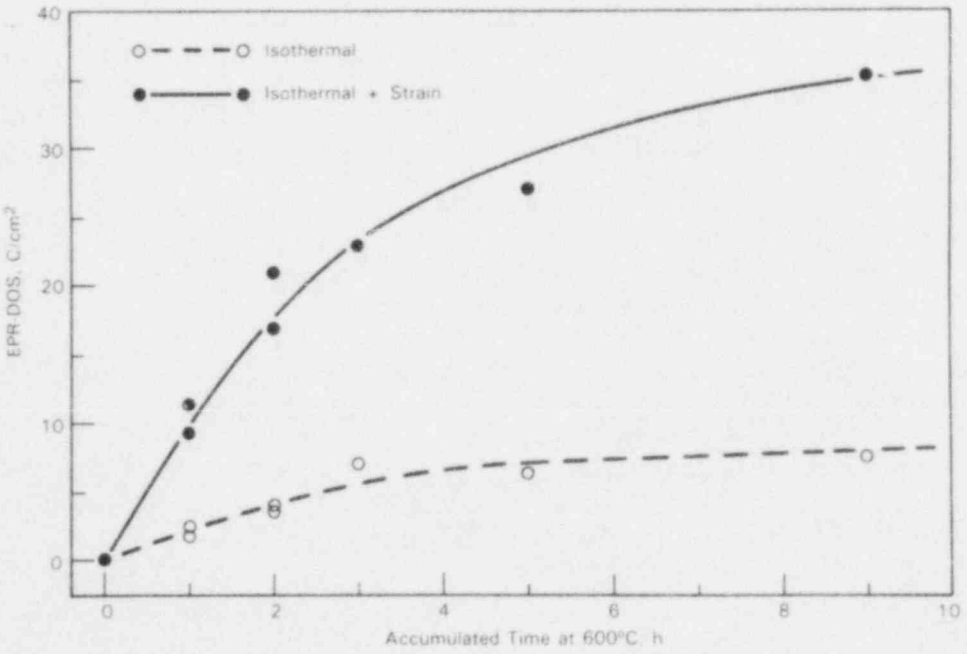

(b)

FIGURE 24. Effect of Simultaneous Deformation on Sensitization Development at 600°C in Two Type 304 SS Heats: (a) C7--0.072 wt% C and (b) C6--0.062 wt% C.

Bright Field Image

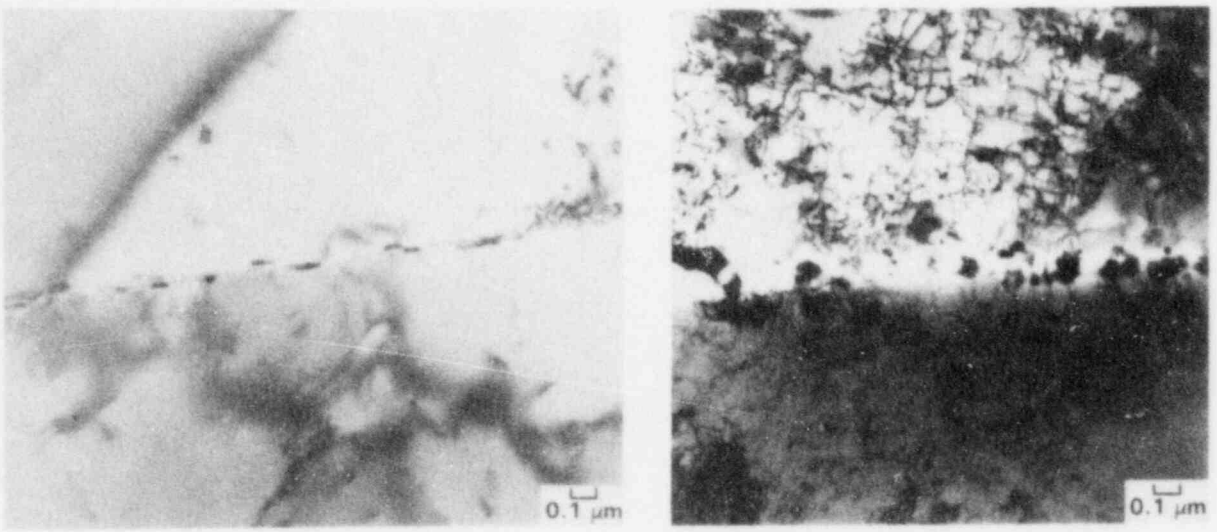

Dark Field Image

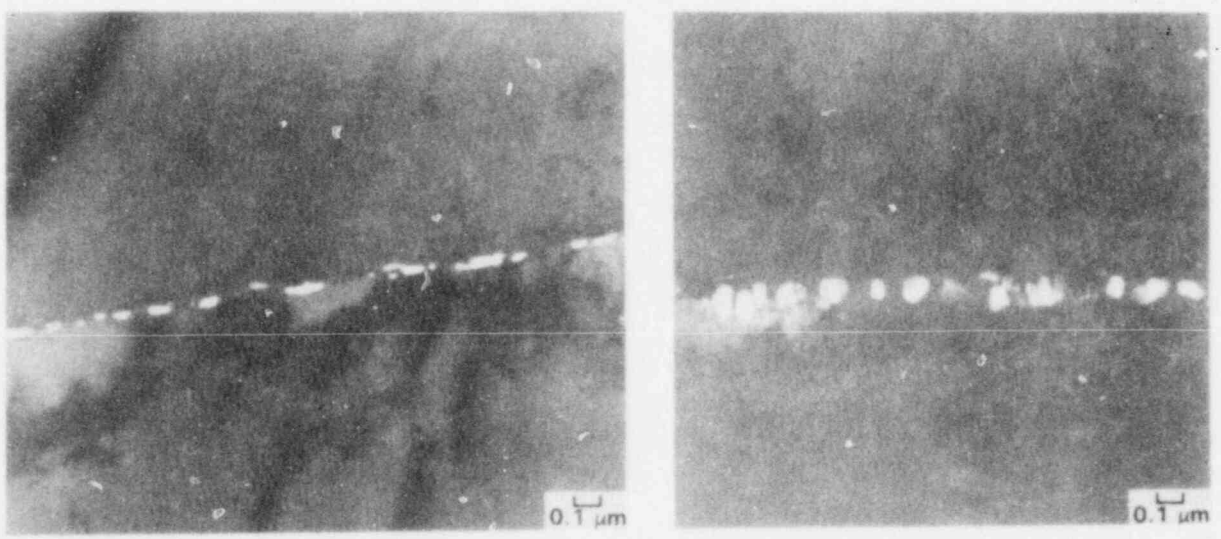

Isothermal

Isothermal + 5% Strain/hr

FIGURE 25. Grain Boundary Microstructures in Unstrained and Strained C7 Specimens After Cumulative Heat Treatment of 9 h at 600°C

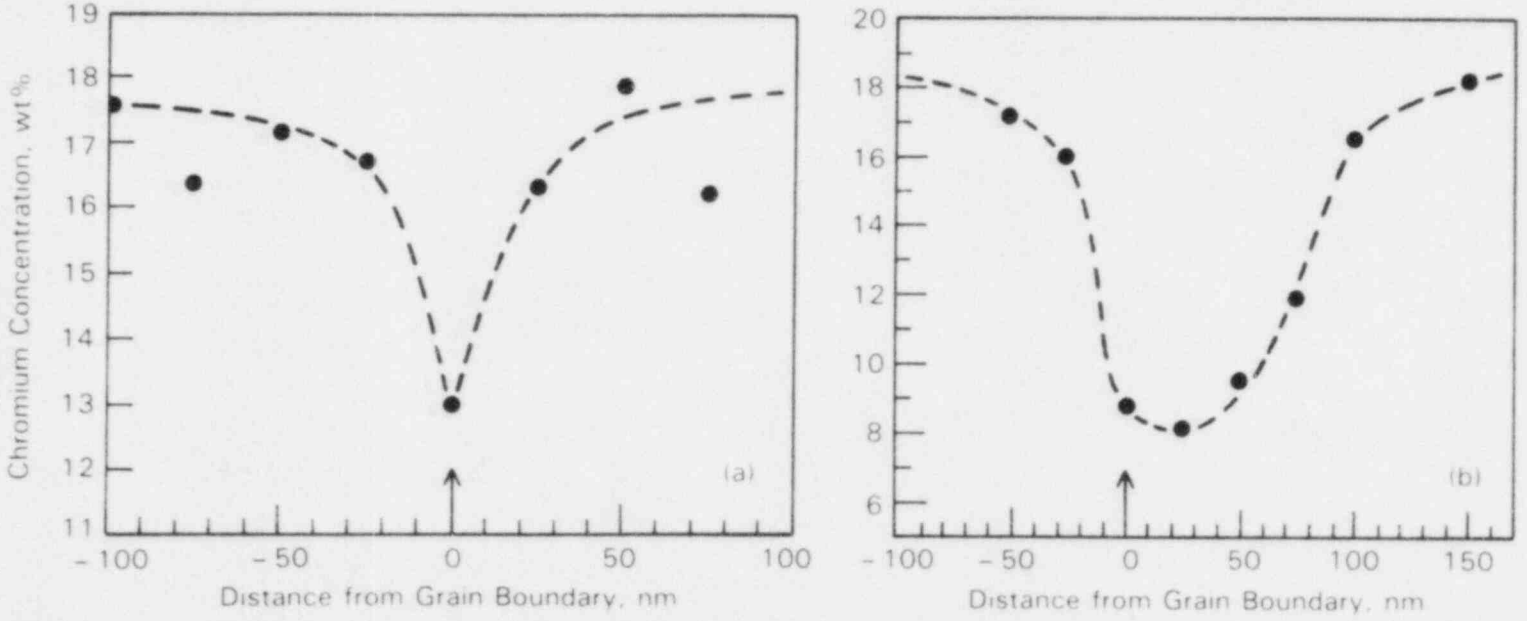

FIGURE 26. Grain Boundary Chromium-Depletion Profiles in Unstrained (a) and Strained (b) C7 Specimens After Cumulative Heat Treatment of 9 h at 100°C

SENSITIZATION DEVELOPMENT IN WELDMENTS

Degree of sensitization measurements have been made on several 24-in.-dia and 14-in.-dia pipe welds as a function of distance through the HAZ using the field cell EPR technique. A detailed mapping of DOS has been conducted after each of the initial twelve passes of the instrumented TM history weld described in Task I. Conditions for the field cell EPR tests are comparable to those described previously[1,2] except that the pipe surface is prepared to a 600-grit finish and pre-etched at a potential of -0.2 V for 30 seconds before establishing the corrosion potential and passivating the surface. These pretreatments eliminate the need to diamond polish the specimen surface.

Variations in DOS through the HAZ have been mapped using several different analysis areas. The smallest analysis area used, which still gives reproducible results, was found to be 0.1 cm by 0.4 cm. More commonly, a mask, 0.1 cm by 0.6 cm, is used to map the HAZ in 0.1-cm steps. A large mask, 0.4 cm in diameter, is also used to corroborate the small-area results. Care must be exercised with the small mask to ensure that preferential attack has not occurred at or under the edges of the mask. Data scatter in the small-area measurements is greater than scatter using the larger area or in laboratory tests. Typically repetitive measurements are within ±20% for the smaller area compared to ±10% for the larger area. An average of three tests is reported.

Examples of DOS mapping through a weldment HAZ are shown for the 24-in.-dia TM history weld in Figure 27. Data for seven of the first eight passes document the increase in DOS with weld pass. The large-area EPR measurements are plotted in Figure 27a and the small area measurements in Figure 27b. Differences in DOS values between the two tests primarily result from the larger area averaging over the higher EPR-DOS regions. In both cases DOS is relatively low until Passes 5 and 6, where levels increase to near the maximum. No significant changes in DOS are observed after Pass 8.

Several other HAZs have been mapped after welding. Consistent with 24-in.-dia TM history weld, a maximum DOS has been observed at a distance between 0.1 and 0.4 cm from the fusion line. The extent of the sensitized region and the maximum DOS value varies considerably depending on welding parameters.

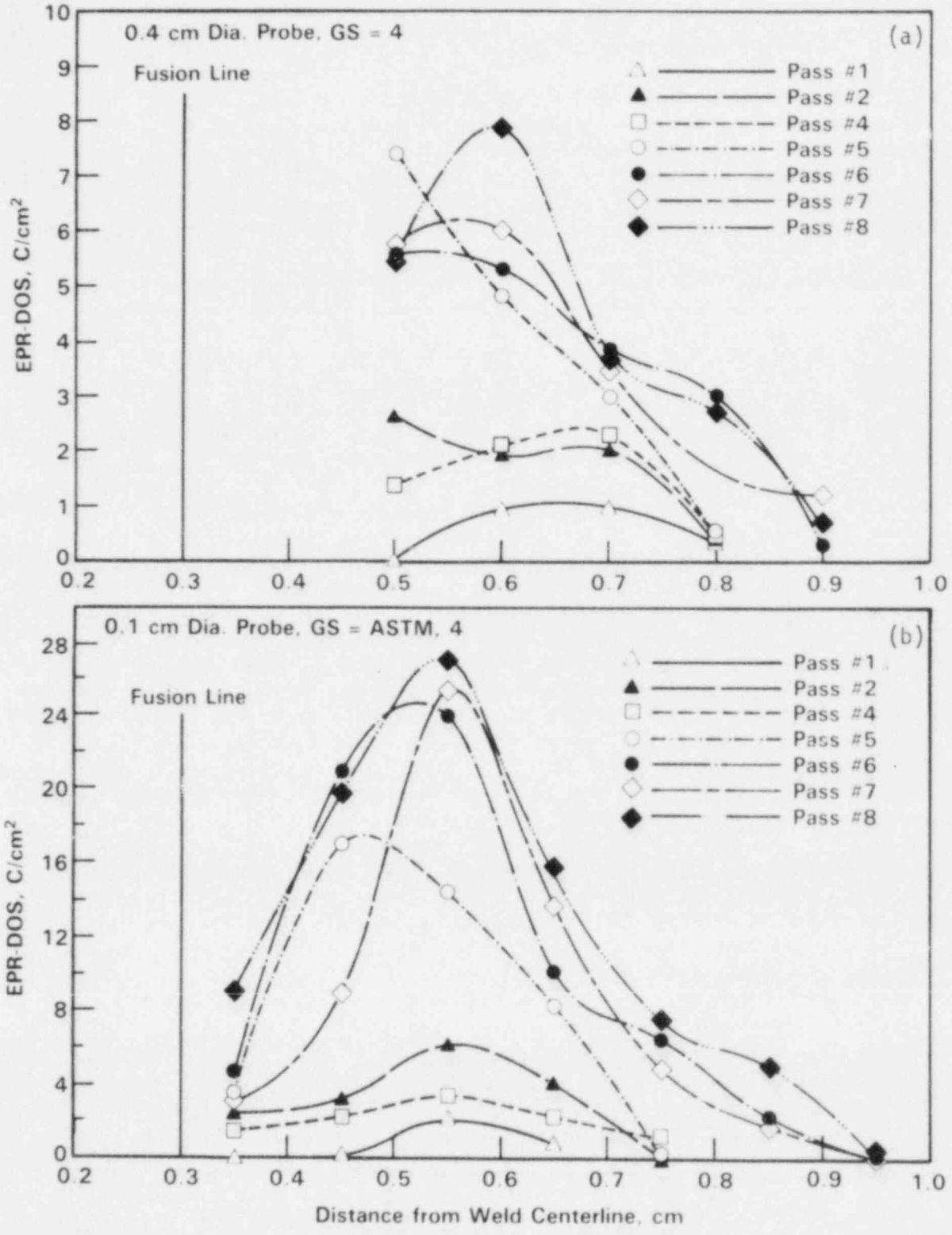

FIGURE 27. Sensitization Development in the HAZ of the 24-in.-dia TM History Weld Using the Large-Area (a) or Small-Area (b) Field Cell EPR Technique

TASK III: SCC PREDICTION FROM COMPONENT-SPECIFIC THERMOMECHANICAL HISTORIES

Austenitic SS components of commercial BWRs and PWRs have experienced SCC in the HAZ of SS welds in service. This type of cracking phenomenon can result in serious component failure. Extensive research over the last several decades has defined the factors controlling SCC: susceptible microstructure, tensile stress, and an aggressive environment. However, at present, SCC susceptibility of in-service weldments can be predicted only qualitatively.

The objective of this task is to develop and validate a methodology to quantitatively predict the SCC susceptibility of HAZ regions in austenitic SS weldments. The basic methodology will include:

- TM history prediction from welding and/or repair-welding parameters
- Microstructural development prediction from TM history and from material composition and condition
- SCC susceptibility prediction from material composition and condition, from TM history and from microstructure.

Each of these steps will be assessed by direct comparison to the experimental data base generated in Tasks I and II. Models will be developed, evaluated, and modified (where appropriate) to best predict the overall data base.

QUANTITATIVE MODELING OF SENSITIZATION DEVELOPMENT

A model for the prediction of material DOS as a function of bulk composition, initial condition, and TM history is being developed. Basic components of the model include determination of the equilibrium chromium concentration at the carbide-matrix interface based on the thermodynamics of carbide formation, chromium concentration gradients based on "effective" diffusivities, and an empirical correlation between chromium depletion and DOS as measured by the EPR test. Empirical correlations also present in the model adjust composition bulk diffusion, and the onset and progression of healing during extended heat treatment.

The DOS predictive model is currently written in BASIC to run on a personal computer. Sections of the current version require input of material composition (Ni, Cr, C, Mo, and N), material condition (mill annealed or solution annealed), and selected material properties, including any prior EPR-DOS value. Choices can be made concerning isothermal exposure, linear continuous cooling, and the effect of simultaneous strain on the DOS prediction. The computation sections of the model include a thermodynamic calculation to define chromium concentrations at the carbide/matrix interface for each temperature and a kinetic calculation to define, through conventional chromium diffusion analysis, the depleted zones as a function of time and temperature. The initially developed model used data for the thermodynamics and diffusivities for austenitic SS appearing in the literature. As the experimental and literature data base has increased, the model has been empirically adjusted.

An important aspect of the model is the prediction of DOS in a form that allows straightforward comparison to experiment. Thus, existing model capabilities and attempts to improve the predictive ability can be evaluated using an inexpensive, yet quantitative technique (i.e., EPR). Sensitization development during isothermal or continuous-cooling heat treatments has been modeled in both Types 304 and 316 stainless steels. Comparisons between measured (Task II) and predicted EPR-DOS values are presented and discussed in the following sections. The final section assesses the ability to predict DOS in an actual pipe weldment by comparison to the results from the 24-in.-dia TM history weld.

CONTINUOUS-COOLING SENSITIZATION PREDICTIONS

Continuous-cooling sensitization is evaluated by using small, additive isothermal time steps to approximate the cooling (or heating) curve. The model requires that information concerning maximum temperature and cooling rates be input. Examples of model predictions illustrating the effect of maximum temperature and cooling rate on DOS are shown in Figure 28. Sensitization increases for all three cooling rates as the maximum temperature is increased to about 800°C. The predicted DOS during a single thermal cycle is constant for maximum temperatures between 800 and 900°C for the slowest cooling rate (0.1°C/s), 800 and 940°C for a rate of 1.0°C/s, and 800 and 975°C for a rate of 10°C/s. At higher temperatures (exact temperature depends on cooling rate as indicated above), DOS begins to decrease until it reaches a value that is constant over some temperature range.

The two plateaus in the curves shown in Figure 28 indicate predictions for mill-annealed (upper) and solution-annealed (lower) material. When high temperatures (>900°C) are reached for a sufficient length of time, the material condition changes from mill annealed to solution annealed. Since the "effective" chromium diffusivity is slower for solution-annealed material, the resultant DOS is smaller. The increase in DOS with maximum temperatures up to about 800°C is due to the fact that sensitization is predicted to occur at temperatures up to 800°C for a heat of this composition. Thus, maximum temperatures below 800°C would have a shorter time in the temperature regime for sensitization and produce a smaller predicted DOS.

Differences in model predictions for mill-annealed and solution-annealed material are also illustrated in Figure 29. Continuous-cooling sensitization measurements from several sources[9-11] have been compiled and compared to model predictions. The curves represent model predictions of the cooling rate required to produce an EPR-DOS value of about 5 C/cm^2. Data points are based on modified Strauss test results with open points showing no attack and closed points showing intergranular attack. Overall prediction trends are quite good, considering that the material used by Hishida and Nakada[9] probably was in the mill-annealed condition (due to a lower-temperature anneal) and the others were in the solution-annealed condition. The data presented in Figure 29 illustrate the effect of bulk carbon content on model predictions.

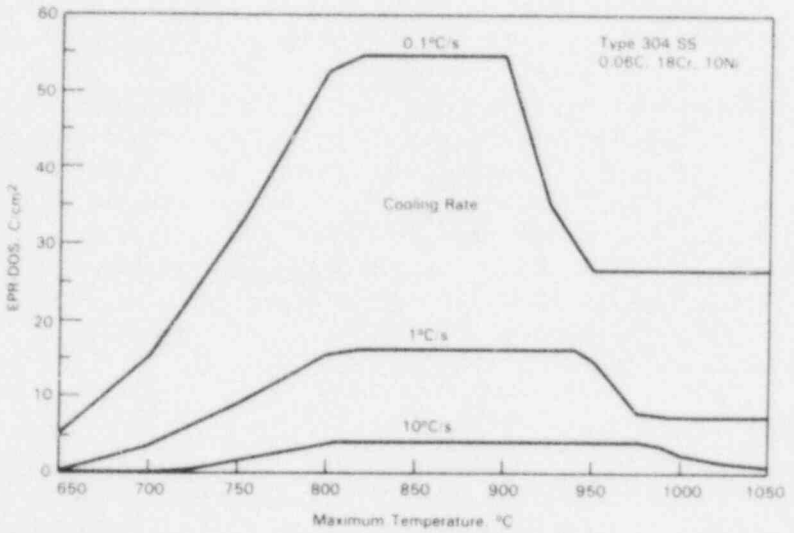

FIGURE 28. Model Predictions of Continuous-Cooling Sensitization Development as a Function of Maximum Temperature During the Cycle for Several Cooling Rates on Mill-Annealed Material

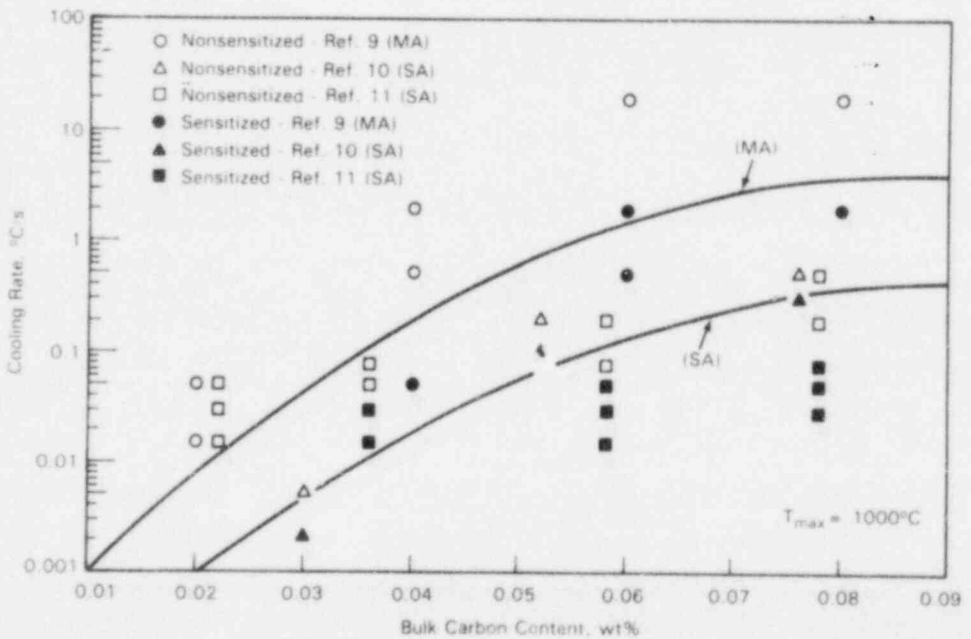

FIGURE 29. Comparison of Model Predictions to Continuous-Cooling Sensitization Data from Several Sources[9-11] for Mill-Annealed (MA) and Solution-Annealed (SA) Type 304 SS Heats

A more detailed assessment of model prediction of sensitization development has been performed by comparison to program continuous-cooling experiments described in Task II. Measured and predicted EPR-DOS for several Type 304 SS heats are presented in Figure 30. In general, predictions reflect sensitization development in the heats. However, agreement with the entire data set is not nearly as good as noted from comparison to isothermal data.[1] This is not unexpected due to the more complex nature of the continuous-cooling thermal treatment and because the model was developed and modified based on primarily isothermal results. Assessment of the continuous-cooling data is continuing along with additional experimentation at different maximum temperatures and cooling rates. It is expected that modifications to the model will be required to better predict the full data base.

HAZ SENSITIZATION PREDICTIONS

Sensitization development in the HAZ of several 14- and 24-in.-dia pipe welds has been modeled. Initial comparisons for the 14-in.-dia weld were discussed in an earlier report.[1] A detailed comparison will be presented here for the 24-in.-dia TM history weld. The 24-in.-dia weld is unique because it was fully instrumented to map pass-by-pass TM history (Task I) with DOS measured in the HAZ after each pass by EPR (Task II). Thus, an accurate pass-by-pass data set is available for direct comparison of experiment and model prediction.

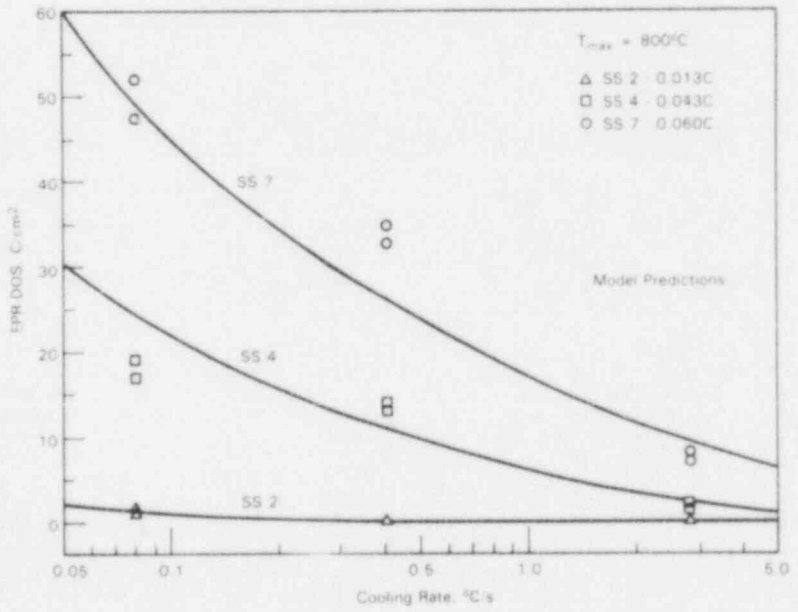

FIGURE 30. Measured and Predicted Sensitization Development in Type 304 SS as a Function of Cooling Rate During Continuous-Cooling Sensitization

Thermal history data from HAZ thermocouples were compiled during heating and cooling for each location and input for model predictions. A gradual increase in DOS is predicted from Passes 1 through 5 as illustrated in Figure 31a. Predictions are only made at thermocouple locations of 0.38, 0.51, 0.64, and 0.77 cm from the weld centerline. Extrapolation of thermal input between these data points was not done, but it appears that maximum DOS occurs between 0.5 and 0.6 cm due to the balance between maximum temperature and cooling rate.

Model predictions are assessed by comparison to a "composite" of the experimentally measured DOS after each pass (Figure 31b). This composite profile incorporates an analysis of both the small- and large-area EPR data from Figure 28. Good agreement can be seen in the location of maximum DOS and the shape of the DOS versus HAZ location curves. Final measured DOS levels are somewhat higher (~25%) than predicted levels. Differences might be even greater if the model did not overpredict the first few passes. Overall, however, the correlation between prediction and experiment is promising considering the model data base to date has primarily been isothermal sensitization data. The overprediction during the early passes reflects the need for a better treatment of precipitate nucleation in the model for continuous-cooling thermal cycles. The final underprediction of DOS results in part from neglecting the effect of deformation during the thermal cycle. If, for example, empirical correlations based on the isothermal strain effects on sensitization experiments (Task II) are used to accelerate sensitization kinetics, simultaneous strains of 1% to 2% during each pass will give predictions comparable to those measured. Preliminary analysis of measured displacements in the HAZ during each pass indicates such strains are produced. Model modification and analysis of these data are continuing.

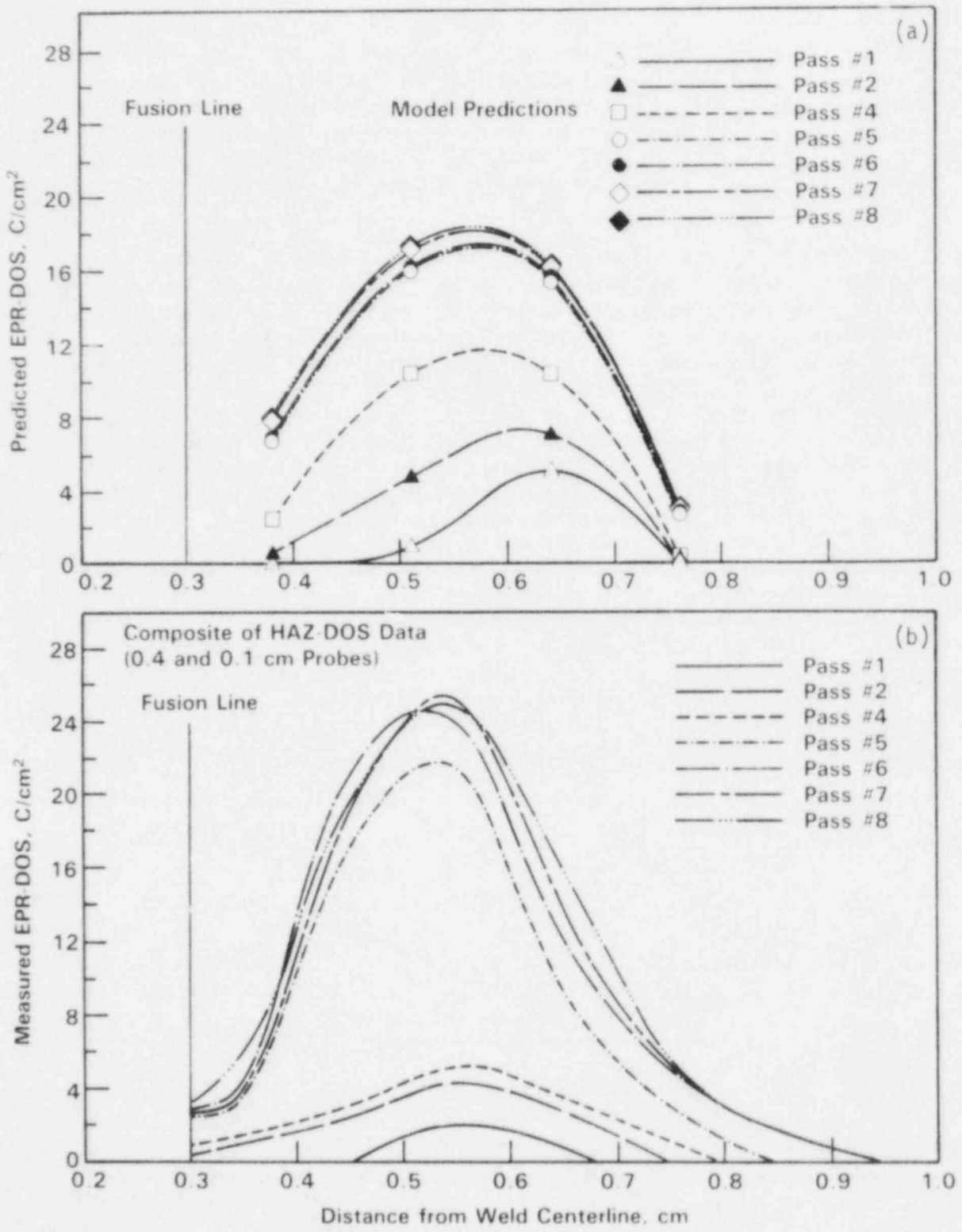

FIGURE 31. Sensitization Development in the HAZ of the 24-in.-dia TM History Weld: (a) Model Predictions and (b) Experimental Measurements

REFERENCES

1. D. G. Atteridge, R. E. Page, and S. M. Bruemmer. 1985. Evaluation of Welded and Repair-Welded Stainless Steel for LWR Service--Annual Report for 1984. NUREG/CR-3613-2, prepared for the Nuclear Regulatory Commission by Pacific Northwest Laboratory, Richland, Washington.

2. S. M. Bruemmer. 1985. "Composition-Based Correlations to Predict Sensitization Resistance of Austenitic Stainless Steels." Paper 106 presented at CORROSION/85, National Association of Corrosion Engineers, Houston, Texas.

3. W. L. Clarke. 1976. The EPR Method for the Detection of Sensitization in Stainless Steels. NUREG/CR-1095, U.S. Nuclear Regulatory Commission, Washington, D.C.

4. W. O. Binder, C. M. Brown and R. Franks. 1949. Trans. ASM 41:1301.

5. C. L. Briant, R. A. Mulford, and E. L. Hall. 1982. Corrosion 38(9):468 and 39(4):132.

6. W. A. T. Clark, T. Arul Mozhi, and D. D. MacDonald. 1983. Influence of Nitrogen on the Sensitization, Corrosion, Mechanical and Microstructural Properties of Stainless Steels--2nd Annual Report. DOE/ER/10972-T2.

7. S. M. Bruemmer, L. A. Charlot, and D. G. Atteridge. 1984. Compositional Effects on the Sensitization of Austenitic Stainless Steels. NUREG/CR-3918, prepared for the Nuclear Regulatory Commission by Pacific Northwest Laboratory, Richland, Washington.

8. G. Cliff and G. W. Lorimer. 1972. Proceedings of the Fifth European Congress on Electron Microscopy. Institute of Physics, Bristol, p. 140.

9. M. Hishida and H. Nakada. 1978. Corrosion 34(10):338.

10. H. D. Solomon and D. C. Lord. 1980. Corrosion 36(8):395.

11. B. Baroux, M. C. Orlandi, and P.H. Maitrepierre. 1984. Sensitization of Continuously Cooled Austenitic Stainless Steels. The Metals Society, p. 378.

DISTRIBUTION

No. of Copies

OFFSITE

U.S. Nuclear Regulatory Commission
Division of Technical Information and Document Control
7920 Norfolk Avenue
Bethesda, MD 20014

20 J. Muscara
Materials Engineering Technology Division
Nuclear Regulatory Commission
Mail Stop 5650NL
Washington, DC 20555

E. F. Rybicki
Mechanical Engineering Dept.
University of Tulsa
600-South College Ave.
Tulsa, OK 74104

H. D. Solomon
Materials Characterization Laboratory
Corporate Research & Development
General Electric Company
P.O. Box 8
Schenectady, NY 12301

W. E. Wood
Oregon Graduate Center
19600 N.W. Walker Road
Beaverton, OR 97006

No. of Copies

C. L. Briant
General Electric Company
Research and Development Center
Schenectady, NY 12301

E. Merrick
Division of Engineering Design
Tennessee Valley Authority
400 Commerce Avenue
W10-B119C-K
Knoxville, TN 37902

W. J. Shack
Materials Science Division
Argonne National Laboratory
9700 South Cass Avenue
Argonne, IL 60439

J. Y. Park
Materials Science Division
Argonne National Laboratory
9700 South Cass Avenue
Argonne, IL 60439

P. S. Maiya
Materials Science Division
Argonne National Laboratory
9700 South Cass Avenue
Argonne, IL 60439

W. L. Clarke
Vallecitos Nuclear Center
Mail Code V36
Pleasanton, CA 94566

No. of
Copies

J. D. Gilman
Nuclear Power Division
Electric Power Research
Institute
3412 Hillview Avenue
Palo Alto, CA 94304

W. J. Childs
Nuclear Power Division
Electric Power Research
Institute
3412 Hillview Avenue
Palo Alto, CA 94304

K. W. Mahin
Lawrence Livermore Laboratory
University of California
P.O. Box 808
L-2A
Livermore, CA 94550

D. Cubicciotti
Nuclear Power Division
Electric Power Research
Institute
3412 Hillview Avenue
Palo Alto, CA 94304

J. F. Key
Fuels & Materials Division
EG&G Idaho, Inc.
P.O. Box 1625
Idaho Falls, ID 83401

R. Horn
General Electric Company
Nuclear Energy Engineering
Division
175 Curtner Ave.
San Jose, CA 95125

J. B. Haworth
Electralloy Corporation
475 Park Avenue South
New York, NY 10016

No. of
Copies

E. A. Loria
Universal-Cyclope Specialty
Steel Division
Bridgeville, PA 15017

P. Lindsey
Bechtel Power Corporation
Mail Stop 52/6/B/6
50 Beale Street
San Francisco, CA 9119

C. D. Lundin
Metallurgical Engineering
University of Tennessee
Knoxville, TN 37916

K. Mosubuchi
Department of Ocean Engineering
Massachusetts Institute of
Technology
Cambridge, MA 02139

ONSITE

45 Pacific Northwest Laboratory

W. E. Anderson
B. W. Arey
D. G. Atteridge (10)
S. M. Bruemmer (10)
L. A. Charlot
R. A. Clark
E. L. Courtright
C. R. Hann
P. E. Hart
E. I. Husa
R. H. Jones
R. S. Kemper (2)
R. F. Klein
B Norton
R. E. Page (2)
J. P. Pilger
F. A. Simonen
P. L. Whiting
Publishing Coordination (2)
Technical Information (5)

*U.S. GOVERNMENT PRINTING OFFICE: 1985-461-721:20304

NRC FORM 335 (2-84) NRCM 1102, 3201, 3202

U.S. NUCLEAR REGULATORY COMMISSION

BIBLIOGRAPHIC DATA SHEET

SEE INSTRUCTIONS ON THE REVERSE

1. REPORT NUMBER (Assigned by TIDC, add Vol. No., if any)
NUREG/CR-3613
PNL-4941
Vol. 3, No. 1

2. TITLE AND SUBTITLE
Evaluation of Welded and Repair-Welded Stainless Steel for LWR Service
Semiannual Report for October 1984 Through March 1985

3. LEAVE BLANK

4. DATE REPORT COMPLETED
MONTH: August
YEAR: 1985

5. AUTHOR(S)
D. G. Atteridge
S. M. Bruemmer
L. A. Charlot
R. E. Page

6. DATE REPORT ISSUED
MONTH: September
YEAR: 1985

7. PERFORMING ORGANIZATION NAME AND MAILING ADDRESS (Include Zip Code)
Pacific Northwest Laboratory
P. O. Box 999
Richland, WA 99352

8. PROJECT/TASK/WORK UNIT NUMBER

9. FIN OR GRANT NUMBER
B2449

10. SPONSORING ORGANIZATION NAME AND MAILING ADDRESS (Include Zip Code)
Division of Engineering Technology
Office of Nuclear Regulatory Research
U.S. Nuclear Regulatory Commission
Washington, DC 20555

11a. TYPE OF REPORT

b. PERIOD COVERED (Inclusive dates)
October 1984 to March 1985

12. SUPPLEMENTARY NOTES

13. ABSTRACT (200 words or less)

Pacific Northwest Laboratory, under the sponsorship of the Division of Engineering Technology of the U.S. Nuclear Regulatory Commission, is conducting a program to determine a method for evaluating welded and repair-welded stainless steel (SS) piping for light-water reactor service. Validated models, based on experimental data, are being developed to predict microstructural development (e.g., the degree of sensitization) and the stress-corrosion cracking (SCC) resistance in the heat-affected zone of the SS weldments. Stress-corrosion cracking is caused by a combination of a susceptible microstructure, an aggressive environment, and tensile stress. Control of any of these three factors can eliminate SCC in most practical situations.

This program will measure and model the development of a susceptible microstructure as it pertains to welded and repair-welded SS pipe. Empirical correlations between material microstructure and SCC will be determined using constant extension rate tests. The successful completion of these tasks will result in a method for assessing the effects of welding/repairing parameters on the SCC resistance of component-specific nuclear reactor welds/repairs.

The present report describes the progress of these studies during the first half of the 1985 fiscal year.

14. DOCUMENT ANALYSIS - a. KEYWORDS/DESCRIPTORS
austenitic stainless steel
intergranular stress corrosion cracking
heat affected zone
degree of sensitization
thermomechanical history

b. IDENTIFIERS/OPEN-ENDED TERMS

15. AVAILABILITY STATEMENT
Unlimited

16. SECURITY CLASSIFICATION
(This page)
Unclassified
(This report)
Unclassified

17. NUMBER OF PAGES

18. PRICE

UNITED STATES
NUCLEAR REGULATORY COMMISSION
WASHINGTON, D.C. 20555